The Fine Structure of K-Series X-Ray Emission Spectra of the Elements Mn (25)-Zn (30) and Ge (32)

The Fine Structure of K-Series X-Ray Emission Spectra of the Elements Mn (25)—Zn (30) and Ge (32)*

Isao EDAMOTO

(Received April 8, 1950)

Synopsis

The fine structure of the x-ray emission spectra $K\alpha$ and $K\beta$, obtained by bent crystal spectrographs, of the elements Mn (25)~Zn (30) and Ge (32) were microphotometrically investigated, and the wave-lengths of many weak lines have been determined. The measurement of the intensity distributions of these spectra was also carried out by the photogram-microphotometer method, and it has been confirmed that the accuracy of the results is comparable to that obtained by the double crystal spectrometer. Next, resolutions of the lines $K\alpha_1$, $K\alpha_2$ and $K\beta_{1,3}$ into their component lines were tried. In consequence, it has been shown that the structures of these lines may be considered to have some correlation with one another.

The use of the net planes which give rise to reflections of large dispersion and an auxiliary lens which reduces the photographic grain effect on the microphotometric curve facilitated the performance of this experiment.

I. Introduction

The present author took a photogram of $K\beta$ spectrum of Cu in 1934 and investigated it microphotometrically in co-operation with Mr. M. Ogura, who then was studying in the author's laboratory, found that there seemed to exist three weak lines on the long wave-length side of $K\beta_1$, and two on the short side of $K\beta_5$, and set about this experiment in 1936 with a view to assure the result of the foregoing experiment and to confirm if there exist the similar lines in the spectra of the elements neighbouring with Cu in atomic number. In the early stage of experiment, on account of the grain effect of photographic film on the microphotometric curve, the detection of weak lines was very difficult and, though it seemed for a time even impossible, the expected purpose was achieved at length by succeeding in designing and grinding out an auxiliary lens for a microphotometer which serves to diminish the grain effect on one side, and by the refining and

* The 588th Report of the Research Institute for Iron, Steel and Other Metals.

improvement of spectrographs on the other.

Further, with the progress of experiment the intensity measurement of spectra was carried out, and the result comparable with that of a double crystal spectrometer was obtained. So the separation of $K_{\beta_{1,3}}$ doublet was tried on the basis of this experiment. As the consequence, we believe, it may be interpreted that there exists a correlation among the asymmetric structures of K_{α_1}, K_{α_2} and $K_{\beta_{1,3}}$ doublets. At the same time it may be regarded that the component lines obey the classical dispersion formula, and the reasonable determination of the relative intensities of component lines is possible on this assumption for the first time.

II. Apparatus employed and preliminary investigations

1. Apparatus employed

(a) The spectrograph

Three spectrographs (I, II and III), each of Johann's type[1], were used. The spectrograph of this type is, as well known, constructed as to reflect the x-ray with a thin crystal plate which is generally cut out parallell to a net plane of the crystal and bent so as to form a cylindrical surface. When the crystal plate C is bent in a cylindrical surface of a radius $2R$ as shown in Fig. 1, then the reflected beams focus on a circle 0 having a radius R. If the source of x-ray be at the point S on this circle, then the beams of the wave-length that satisfies the Bragg's equation focus, after diffracted by the crystal, to the point S_1, the symmetry point of S with respect to the symmetry plane parallel to the generating lines of the cylindrical surface. But when the focus of an x-ray tube is set in the position S, the width of the spectrum obtained at S_1 is not larger than that of the focus of the tube, hence it is preferable to put the x-ray source between S and C to take a photogram for a wide range of spectrum at the same time. In Fig. 1 H_1, H_1' indicate the crystal holder; H_2 the plate holder; D_1 and D_2 the divided circles. The crystal plate used is a quartz plate of Y-cut (see Fig. 2) having the thickness of 0.2~0.3 mm, bent about an axis parallel to the optical axis.

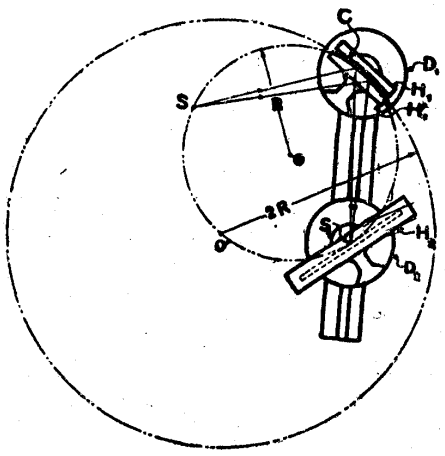

Fig. 1. A rough sketch of the spectrograph.

Spectrograph I.

(1) H. H. Johann, ZS. f. Phys. **69** (1931), 185.

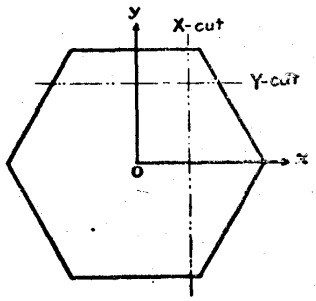

Fig. 2. The names of cuts of a quartz.

This spectrograph is of a very simple construction having no divided circle nor a scale to measure the distance from the crsytal to the plate. The crystal plate used is of Y-cut, and the face to be exposed to x-rays is polished optically flat. The crystal holder is made of brass, and the diameter of the focusing circle is about 52 cm. This spectrograph, though simple, well serves the precise measurement of wave-length by using three spectral lines of known wave-lengths as reference lines as will be related in 4, (iii) of this chapter.

Spectrograph II.

This spectrograph is provided with the divided circles D_1 and D_2 whose verniers enable us to read the angles to 3 minutes, and the distance from the crystal to the plate may be read by a scale attached to the bench of the spectrograph. The quartz plate used is also of Y-cut in this case, having its surface etched with hydrogen fluoride for a minute after being ground with very fine grains of carborundum in plane. This quartz plate and the one used for the next following spectrograph, III, are such that their finished surfaces are parallel to the net planes of the crystal within the error of one minute. These quartz plates are kindly prepared by Prof. I. Koga and Assist. Prof. M. Tachibana both then in the Tokyo Technological College, and by these the writer accepted a great deal of convenience for the performance of this experiment. The crystal holder used in this spectrograph is made of slate and was manufactured by the writer by the method described in 2 of this chapter and its focusing circle is about 51.4 cm in diameter.

Spectrograph III.

This spectrograph is quite the same as the spectrograph II except that it is a large sized spectrograph of the focusing circle of about 153 cm in diameter and that the quartz plate of X-cut is used.

(b) X-ray tube

Two x-ray tubes, Siegbahn-Hadding type and Sandström type, were used as the sources of x-rays. The former has three windows and x-rays emitted from the two of them were used as the sources for the spectrograph I and III; while the latter tube was used as the source for the spectrograph II alone. For both tubes, the high tension currents were supplied from 50~single phase transformers rectified through kenotrons in half waves. Applied voltages were 20~25kV in effective value, and the currents were 10~15 mA.

The targets used in the present experiments were metal plates of 1 mm in thickness soldered on the copper anticathode except Mn and Ge. These

elements were used as fine powder, rubbed onto a roughened copper plate of 1mm thickness which was soldered on the copper anticathode.

2. Preparation of the crystal holder

The crystal holder used in the spectrograph III ought to be made as to form a cylindrical surface of 300 cm in diameter. The writer was obliged to make by himself and constructed a device of grinding out the cylindrical surface (Fig. 3).

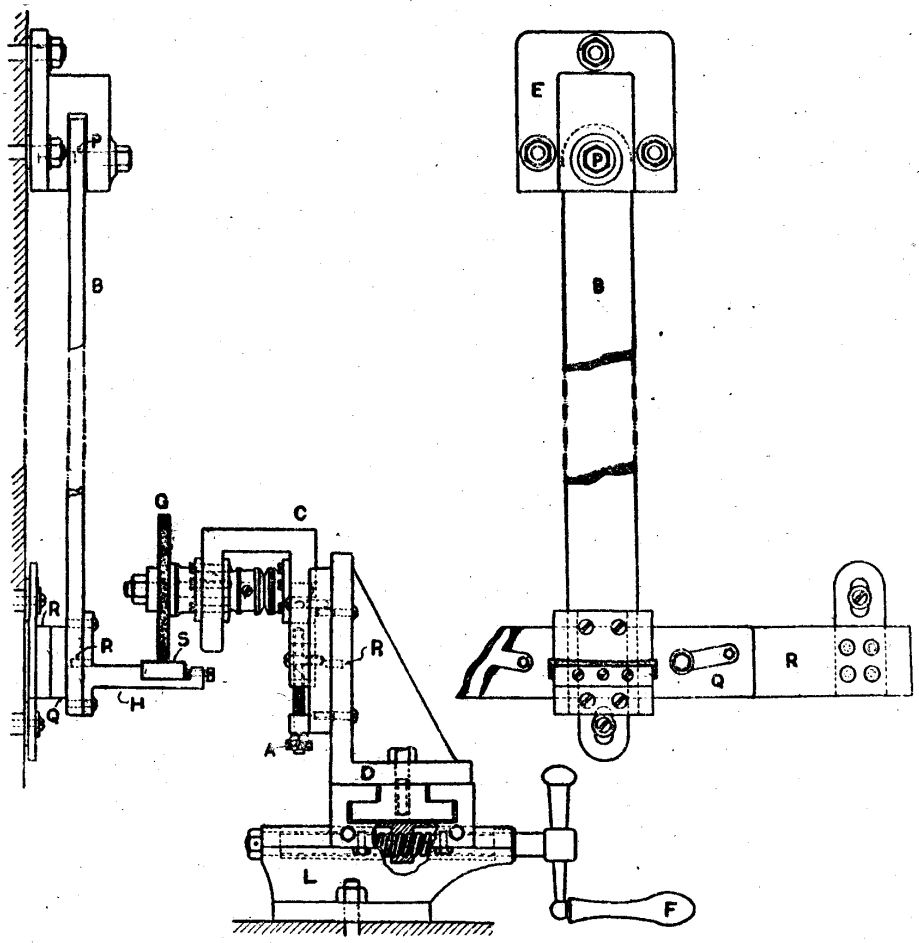

Fig. 3. Device of grinding out the cylindrical surfaces of a crystal holder.

A piece of slate (S in the fig.), of which the crystal holder was made, was settled onto the frame H, and H was fixed by four screws on the bar B which can be swung in a vertical plane, like a pendulum, about the axis of a pin P, keeping sliding contact of the metal plate Q, attached to B, on the metal plate R fixed on the wall. To grind a cylindrical surface was employed the grinding wheel G, driven by a motor. The height of G may be adjusted by the screw A attached to the guide plate C, while L, a part of a lathe, on which D, the bench of G, is mounted, permits G to shift in the direction normal to the wall by means of the

handle F. Consequently, by a slow swinging motion of B, the concave surface of the holder may be ground out, step by step, for each slightly nearer position of G. During this procedure two pins P_1 and P_2, and the lowest boundary of G ought to be so kept as they lie in a horizontal plane. To grind the convex cylindrical surface of the holder, after replacing S with the other piece of slate which makes a pair with S, and turning H and C by 180° about the axis of P_1 and P_2 respectively, similar procedure as above will do. A pair of cylindrical surfaces so ground are smoothened by rubbing each other with water and adhered closely with bee-wax, then the windows for the entrance and exit of x-ray and holes for screws to fasten the quartz plate are cut through. The crystal holder was prepared in this way (Fig. 4).

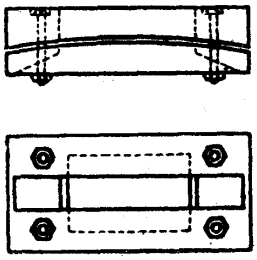

Fig. 4. The crystal holder.

Four pieces of bars B having the length, from P to P_1, of 150 cm, 75 cm, 50 cm and 25 cm, are provided and bolts to fasten E in suitable position according to the length of the bar used are attached on the wall.

The crystal holder, mounted on the spectrograph II, having $2R=50$cm, also was manufactured by this method.

3. Net planes of quartz available to spectroscopy

For spectroscopic measurements, large dispersion is often required. Now let d be the spacing of the net planes, θ the glancing angle, n the order of reflection and λ the wave-length of the x-ray, then the condition of reflction is given by the equation

$$2d \sin \theta = n\lambda ;$$

hence the dispersion is

$$\frac{d\theta}{d\lambda} = \frac{n\lambda}{2d \cos \theta} \cdot \frac{1}{\lambda} = \frac{1}{\lambda} \tan \theta .$$

Therefore, for the given value of the wave-length λ, the large dispersion may be acquired by the use of reflection of large glancing angle. But since reflections having weak intensities are practically useless though they may have large dispersion, the next experiment was performed to search for the net planes of large dispersions and of strong reflection at the same time. The apparatus employed was the spectrograph II, and the anticathode was of Cu. In the case of a bent crystal spectrograph, on account of

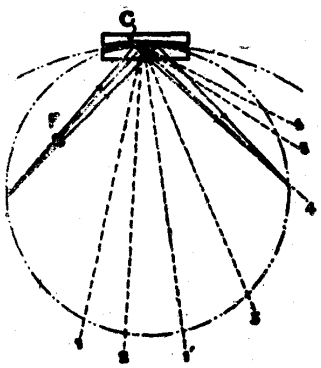

Fig. 5 Directions of strong reflection.

focusing of reflected beams, spectra of strong reflection are well seen through a fluorescent screen. In Fig. 5, rotating the bent crystal C slowly about the axis parallel to the generating lines of it, spectra of strong reflection were observed in the positions **1**, **2**, **1'**, **3**, ... as indicated in the figure.

The net planes which give rise to these reflections were determined. The results are shown in Figs. 6 ~10 with exception of the reflection "**1'**" which was confirmed to be raised by the reflection of Cu$K_{\beta_{1,3}}$ from the same net planes as the reflection "**1**".

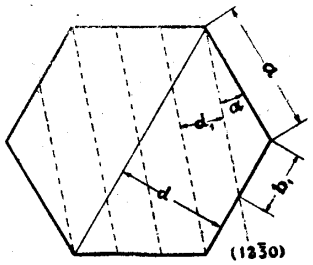

Fig. 6. Net planes raising the reflection "**1**" (24$\bar{6}$0); $a=19°6'23.8''$, $2d_1=3210.42$ XU.

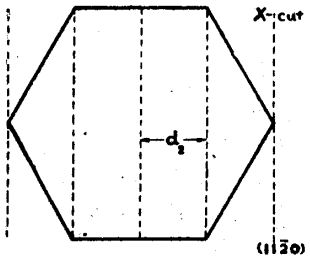

Fig. 7. Net planes raising the reflection "**2**" (33$\bar{6}$0); $a=30°$, $2d_2=4904.02$ XU.

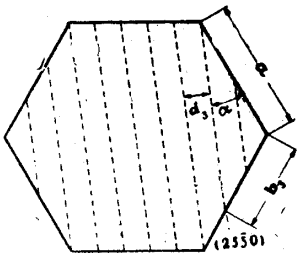

Fig. 8. Net planes raising the reflection "**3**" (23$\bar{5}$0); $a=23°24'48''$, $2d_3=1948.66$ XU.

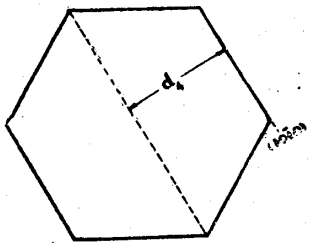

Fig. 9. Net planes raising the reflection "**4**" (40$\bar{4}$0); $a=0°$, $2d_4=8494.00$ XU.

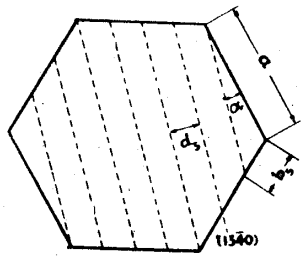

Fig. 10. Net planes raising the reflection "**5**" (13$\bar{4}$0); $a=13°53'52''$, $2d_5=2355.80$ XU.

Now glancing angles θ_{α_1} (Table 1) and $\theta_{\beta_{1,3}}$ (Table 2) for K_{α_1} and $K_{\beta_{1,3}}$ of the elements Cr(24)—Ge(32) for the reflections above-mentioned are shown.

Table 1. Glancing angle θ_{α_1} for K_{α_1}

	(24$\bar{6}$0) Reflection"**1**"	(33$\bar{6}$0) Reflection"**2**"	(23$\bar{5}$0) Reflection"**3**"	(40$\bar{4}$0) Reflection"**4**"	(13$\bar{4}$0) Reflection"**5**"
Cr (24)					75°42′20″
Mn (25)				81° 1′33″	62°48′50″
Fe (26)			82°31′ 6″	65°29′ 6″	55° 1′18″
Co (27)			66°22′23″	57°13′ 6″	49°12′43″
Ni (29)			58° 6′29″	51°10′55″	44°33′36″
Cu (29)	73° 7′13″	70° 8′ 6″	52° 5′16″	46°23′ 7″	40°41′31″
Zn (30)	63° 9′18″	61°10′54″	47°18′19″	42°24′45″	37°24′ 3″
Ga (31)	56°25′14″	54°53′43″	43°20′12″	39° 2′ 1″	34°33′ 5″
Ge (32)	51°13′37″	49°57′32″	39°57′28″	36° 6′38″	82° 3′19″

Table 2. Glancing angle $\theta_{\beta_{1,3}}$ for $K_{\beta_{1,3}}$.

	$(24\bar{6}0)$	$(33\bar{6}0)$	$(23\bar{5}0)$	$(40\bar{4}0)$	$(13\bar{4}0)$
Cr (24)				78°27′50″	61°55′41″
Mn (25)			78° 1′53″	63°51′34″	53°56′37″
Fe (26)			64° 6′15″	55°38′29″	48° 1′26″
Co (27)		81°41′ 0″	56° 6′13″	49°36′53″	43°18′39″
Ni (28)	68°50′34″	66°19′ 3″	50°11′41″	44°49′48″	39°24′43″
Cu (29)	59°56′38″	58°12′17″	45°28′42″	40°51′50″	36° 6′ 4″
Zn (30)	53°38′ 7″	52°15′18″	41°33′16″	37°29′48″	33°14′32″
Ga (31)	48°40′17″	47°30′38″	38°12′46″	34°35′12″	30°44′37″
Ge (32)	44°34′32″	43°34′ 1″	35°19′14″	32° 2′33″	28°32′27″

The wave-lengths adopted in these calculations are those measured by Bearden and Shaw[2].

Among the reflections above-indicated, those especially of interest, because of very large dispersions, are : Fe$K_\alpha(23\bar{5}0)$, Mn$K_\alpha(40\bar{4}0)$, Co$K_\beta(33\bar{6}0)$, Mn$K_\beta(23\bar{5}0)$ and Cr$K_\beta(40\bar{4}0)$.

4. Accurate relative measurements of wave-lengths

Let us consider the relation between the positions of two spectrum lines on a plate and the wave-lengths of these rays in case of taking a photogram on a plate with a bent crystal spectrograph. In Fig. 11, let C be a bent crystal and P a photographic plate. Now supposing a beam AB_0 intersecting at equal angle φ_0 with the tangent plane at A, the midpoint of C, and with the plate surface PE, and another beam AB reflected in a different direction, and denote the angle between AB and AE by φ, $B_0B=l$ and $AB_0=D$, then there exists a relation

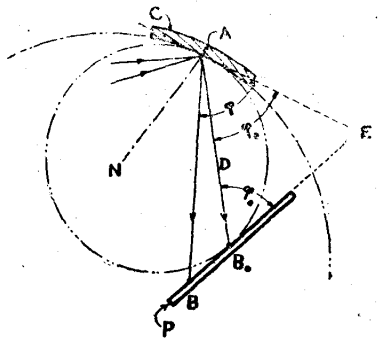

Fig. 11. Method of relative measurement of wave-length.

$$\frac{l}{D}=\frac{\sin(\varphi-\varphi_0)}{\sin(2\varphi_0-\varphi)} \quad \ldots\ldots (1)$$

Further denote the angle between the net plane giving reflection in the direction AB and the face of the crystal by α, the glacing angle for this net plane by θ, the wave-length by λ, the distance between the adjacent net planes by d and the order of reflection by n, then

$$\varphi=\theta+\alpha, \quad \ldots\ldots\ldots\ldots\ldots (2)$$

(2) J. A. Bearden and C. H. Shaw, Phys. Rev. **48** (1935), 18.

and by Bragg's equation

$$2d\sin\theta = n\lambda. \quad \cdots\cdots\cdots\cdots \quad (3)$$

If d, n and α be given, we can find θ and accordingly φ for various values of λ, so that provided previously with a diagram representing the relation between l and λ, measurement of l on the plate permits us to obtain the corresponding value of λ. In this case the absolute measurements of the wave-lengths may be possible. For this purpose, however, very precise measurements of D and φ_0 are required, and accordingly it becomes somewhat difficult problem in practice. But relative measurements may be easily performed in fair accuracy.

Relative measurements are classified in the following three cases.

(i) The case one reference line is used

When the position of B_0 and D are known, and φ_0 alone unknown, then φ_0 can be solved from Eq. (1) by measuring the distance between B_0 and a spectrum line, whose wave-length is known and reflected in the vicinity of B_0. The method of solution is of trial or graphical. Determining φ_0 in this way, wave-lengths of any other spectrum lines can be obtained in like manner as above-mentioned. In the case where D and φ_0 are known and the position of B_0 alone unknown, it is evidently obtainable from Eq. (1).

(ii) The case two reference lines are used

When the position of B_0 and the value of φ_0 are unknown, two spectrum lines of known wave-lengths should be used as the reference lines. Denoting their wave-lengths by λ_1, λ_2; the angles which the reflected beams of these spectra make with the crystal surface by φ_1, φ_2; the distances on the plate from B_0 to the spectrum lines by l_1, l_2, then by Eq. (1)

$$\frac{l_1}{D} = \frac{\sin(\varphi_1-\varphi_0)}{\sin(2\varphi_0-\varphi_1)}, \quad \cdots\cdots\cdots\cdots \quad (4)$$

$$\frac{l_2}{D} = \frac{\sin(\varphi_2-\varphi_0)}{\sin(2\varphi_0-\varphi_2)}, \quad \cdots\cdots\cdots\cdots \quad (5)$$

$$\therefore \quad l_2-l_1 = D\left\{\frac{\sin(\varphi_2-\varphi_0)}{\sin(2\varphi_0-\varphi_2)} - \frac{\sin(\varphi_1-\varphi_0)}{\sin(2\varphi_0-\varphi_1)}\right\} \quad \cdots\cdots\cdots \quad (6)$$

Measuring l_2-l_1, φ_0 can be solved from Eq. (6). And substituting this value of φ_0 into Eq. (4), the value of l_1 is obtained and consequently the position of B_0 is determined.

(iii) The case three reference lines are used

When all of the three, B_0, φ_0 and D are unknown, three reference lines are needed. Denoting the wave-lengths of these spectrum lines by λ_1, λ_2, λ_3; the angles which the reflected beams make with the crystal surface by φ_1, φ_2, φ_3; the distances from B_0 to the spectrum lines by l_1, l_2, l_3, there exists, besides (4) and (5), another to these analogous relation. Accordingly eliminating D between Eq. (6) and an equation analogous to (6), we obtain

$$(l_3-l_2)\left\{\frac{\sin(\varphi_2-\varphi_0)}{\sin(2\varphi_0-\varphi_2)}-\frac{\sin(\varphi_1-\varphi_0)}{\sin(2\varphi_0-\varphi_1)}\right.$$
$$=(l_2-l_1)\left\{\frac{\sin(\varphi_3-\varphi_0)}{\sin(2\varphi_0-\varphi_3)}-\frac{\sin(\varphi_2-\varphi_0)}{\sin(2\varphi_0-\varphi_2)}\right. \quad \cdots\cdots\cdots (7)$$

Measuring l_3-l_2 and l_2-l_1, the value of φ_0 can be obtained by a method of trial or graphically. Substituting this into Eqs. (6) and (4), the value of l_1 accordingly the position of B_0 is determined. Then the wave-lengths of the other spectrum lines are obtained as in the case of (i). Such a procedure provides a fairly precise method of relative measurement even with a spectrograph having neither divided circles nor scale to measure D.

5. Auxiliary lens for microphotometer

In the microphotometric investigation of photographic plates, it is a well known fact that a photometric curve makes itself zigzag, on account of the finite dimension of photographic grains. The present writer, in the investigation of fine structures of x-ray spectra, having been troubled by the grain effect, thought that an apparatus, which acts to elongate the image, projected on the plate, of the slit in the direction of a spectrum line, would be effectual to reduce this effect. An idea of insertion of a cylindrical lens across the path of the ray of light will occur to every one, but an ordinary cylindrical lens inevitably causes distorsion of the elongated image. Exactly longitudinal elongation of the image of the slit, keeping the breadth invariant, will be carried out by the lens mentioned in the following article.

(a) Form of the lens.

The microphotometer used is a Moll-microphotometer Type A manufactured by P. J. Kipp and Zonen. So the following description is confined only in the case of this type, yet the idea will be applicable of course in cases of the other types in like manner.

Figs. 12 (a), (b) show the front view and the plan of the paths of the rays of light from the light source to the thermo-pile of the microphotometer. The image of the filament AB is formed by the lens L_1 on the slit A_1B_1. The rays of light which pass through the slit form the image *ab* of the slit on the film F of the photographic plate P by means of the lens system L_2. The rays of light, after passing through *ab*, form the image A_2B_2 of *ab* on the window of the thermo-pile T by means of the other lens system L_3. In our case, however, the size of the image *ab* on F is about 1 mm in length and about 0.02 mm in width, so, because of the smallness of the area, the entrance and exit of one grain of the photographic film, accompanied by the motion of the plate, fairly affect at once the mean blackness, and corresponding to this, a zigzag appears in the photometric curve. By enlarging the area of the image this effect will be diminished of course, but as the widening of the image is followed by the reduction of the resolving power, the increase of the length alone

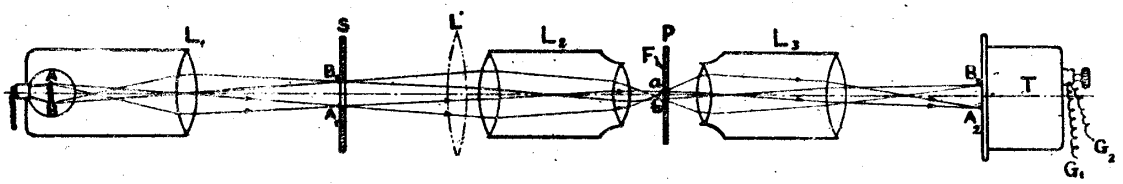

Fig. 12 (a). Paths of the rays of light in the microphotometer (the front view).

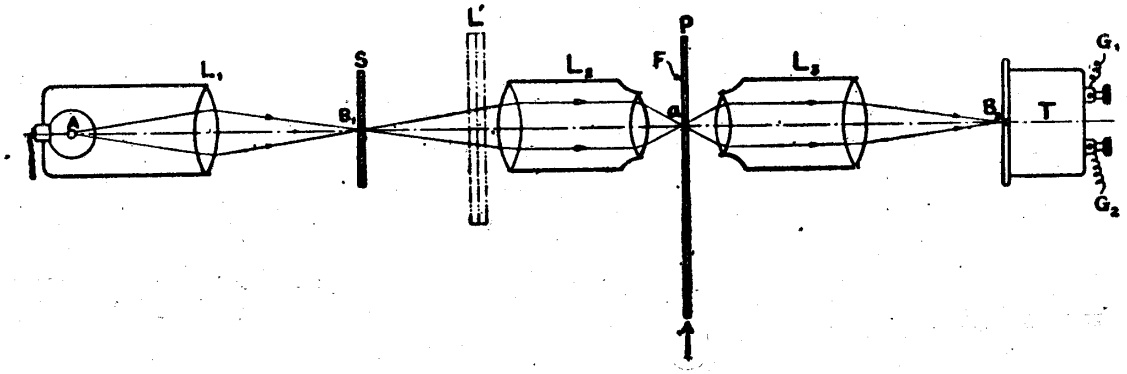

Fig. 12 (b). The same as the above (the plan).

of the image, keeping the width constant, is desirable. Suppose now we bring a cylindrical lens in the position of L′ in Fig. 12 and assume that L′ is bent so that it forms a part of a solid of revolution having the straight line XX′ (see Fig. 14 (a)) —the line coinciding with the longitudinal side A_1B_1 of the slit—as its axis. In other word, we use a lens shaped as a part L′ (Figs. 13 (a) and (b)) of the solid of revolution which is formed by revolving the section C (Fig. 13 (a)), normal to the generating lines, of a cylindrical lens. Accordingly either of the both surfaces of this lens is made of a part of the surface "anchor ring". Fig. 14 shows the case when such a lens is inserted, and (a) the front view, (b) the plan. In this case, the length of the cross section of the beam of light on the plate is, in the front view, elongated, coming to $a'b'$. At the same time, however, the last image comes to $A_2'B_2'$, so that the cross section of the beam at the window of T is also elongated. To compensate this effect, it is sufficed by inserting a lens L″, having similar form as L′, in the position indicated in the figure. Thus the perfect invariance of the width of the beam of light at the window of T is seen evidently in Fig. 14 (b).

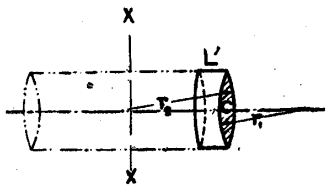

Fig. 13 (a). The form of the auxiliary lens (the front view.)

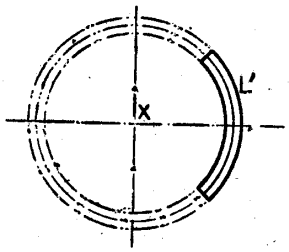

Fig. 13 (b). The same as the above (the plan).

In the writer's case, though he ordered a pair of lenses, shaped as indicated in Fig.

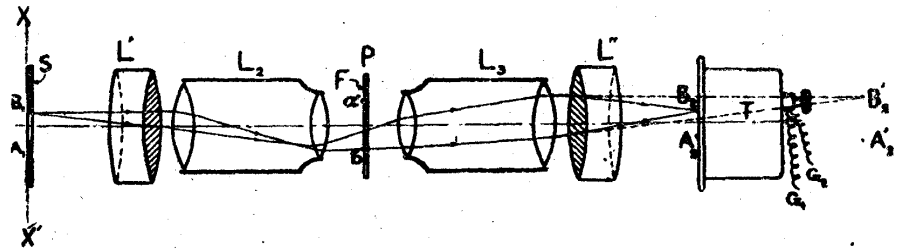

Fig. 14 (a). Paths of the rays of light when the auxiliary lenses are inserted (the front view).

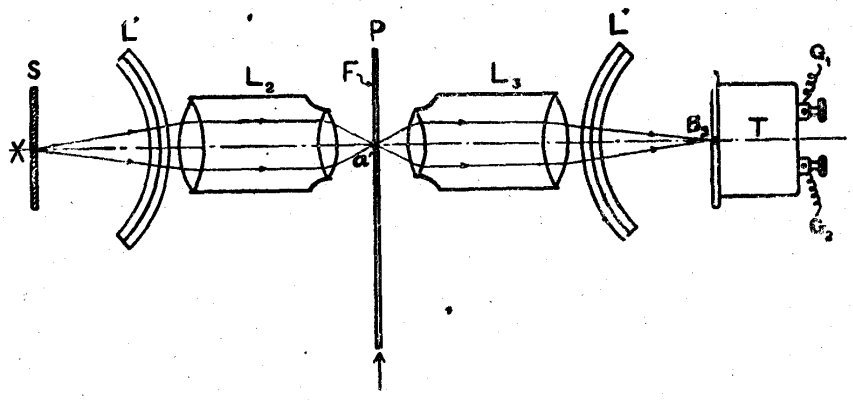

Fig. 14 (b). The same as the above (the plan).

13, to several optical works, none of them made those readily, so the author was obliged to make out by himself, and chose for the convenience of working, as the position for insertion of lenses, the space between L_2 and F, and the space between F and L_3 (Figs. 15 (a), (b)). In this case the suitable form of the lens is such that its section is like that of a concave lens.

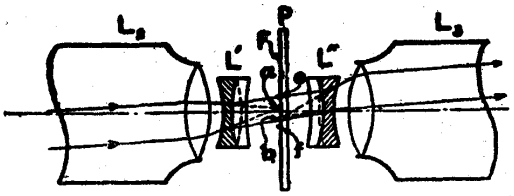

Fig. 15 (a). Form of the image after insertion of the auxiliary lens (the front view).

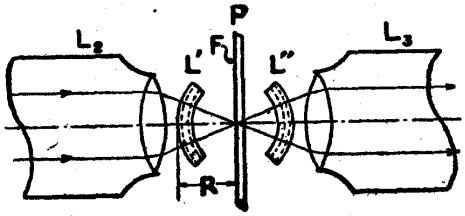

Fig. 15. (b). The same as the above (the plan).

In actual making, a thick glass tube of 14 mm in the outer diameter being fitted on a lathe, ground at first with carborundum cloth, then with emery paper, and polished with colcothar lastly, cut into four pieces and two pieces were used as the lens L' and L''.

(b) Result obtained by the use of the lenses

All the microphotometric curves shown in the following chapter are drawn by using these auxiliary

lenses, and they, becoming very smooth compared with the ordinary ones, facilitated the studying of the structures of spectra.

III. Fine structure of the *K*-series emission spectra

1. Measurement of faint lines in the *K*-series x-ray emission spectra of the elements Mn (25)—Zn (30) and Ge (32)

Investigating the microphotometric curves of spectrum-photograms obtained by the bent crystal spectrographs, many faint lines were detected. At the same time, the measurements of wave-lengths of known faint lines were also carried out, and they were compared with those obtained by using double crystal spectrometers.

(a) Cu K_α

Using the spectrograph II, the photograms of the spectrum arisen by the $(24\bar{6}0)$ reflection were taken. Their microphotometric curves are such that shown in Fig. 16, and besides α_1 and α_2 faint lines are seen at the places marked with $\alpha^{(VIII)}$, α_1', α_1'' and α_2'. Among these the line α_1' is seen directly on the plate separated from α_1. In the figure the places marked with p, q are those where white lines (Aufhellungslinien) running parallel to the spectra were drawn.

The microphotometer employed was, as mentioned already, of the type A manufactured by Kipp-Zonen and the magnification of about 27 times was used.

Next one of the microphotometric curves for which rather long exposures were applied is such that as shown in Fig. 17. Investigating several plates of such photograms, there seemed to exist the faint lines α_3'', $\alpha'\,\alpha''$, α''', $\alpha^{(IV)}$, $\alpha^{(VI)}$, $\alpha^{(VII)}$ besides α_3', α_4 and α_5. To the naked eye are visible the lines α_3', α_4, α_3 of course on the plate, and besides these, some three faint lines are seen in the positions regarded as α'', $\alpha^{(IV)}$ and $\alpha^{(VI)}$. α' is also seemed to be seen though very faint.

To determine the wave-length, using α_1 as the reference line, the value given by Bearden and Shaw[2]

$$\lambda_{\alpha_1}=1537.400\ \text{XU}$$

was adopted as its wave-length, and the method mentioned in II, **4**, (i) was used.

The values of λ thus determined for these lines are shown in the second column of Table 3.

Using the reflection $(40\bar{4}0)$, of the smaller dispersion than the above, a microphotometric curve as shown in Fig. 18 is obtained in the case of long exposure. Investigating similar six plates and fourteen plates of shorter exposure than these, faint lines are seemed to exist in the position α_0'', α_0', $\alpha^{(V)}$, α_2'', α_2''', $\alpha_2^{(IV)}$, $\alpha_2^{(V)}$ and $\alpha_2^{(VI)}$. The wave-lengths for these lines are shown in the third column of Table 3.

As the spectrograph employed is the one which has been denoted as the

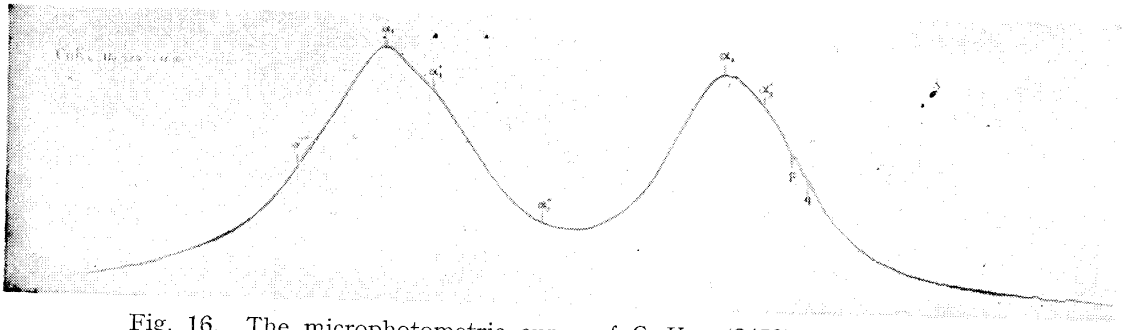

Fig. 16. The microphotometric curve of Cu$K\alpha$—(24$\bar{6}$0) reflection, 5hr 42min ; Spectrograph II.

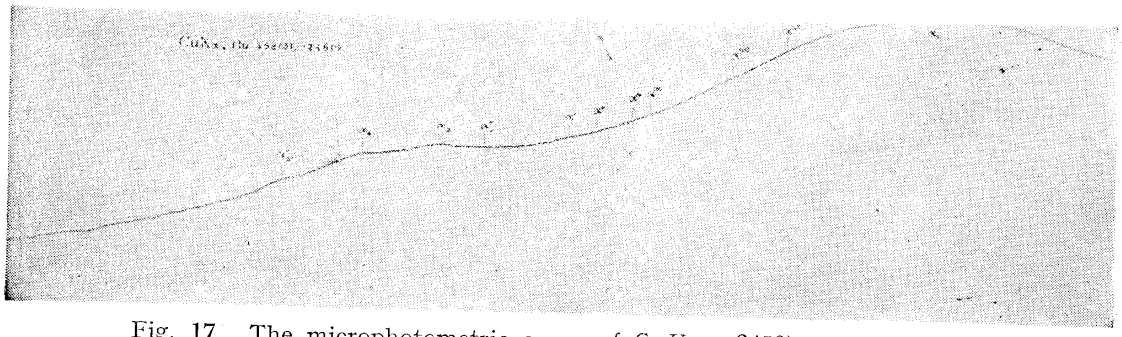

Fig. 17. The microphotometric curve of Cu$K\alpha$—(24$\bar{6}$0) reflection, 19hr 40min ; Spectrograph II.

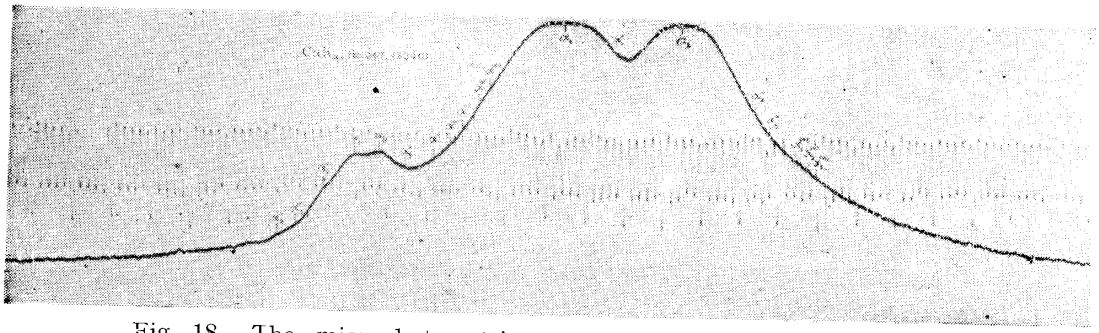

Fig. 18. The microphotometric curve of Cu$K\alpha$—(40$\bar{4}$0) reflection, 37hr 50min ; Spectrograph I.

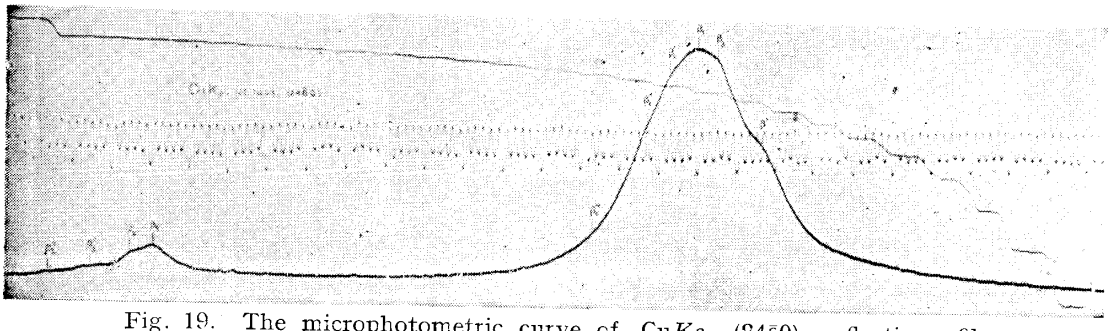

Fig. 19. The microphotometric curve of Cu$K\beta$—(24$\bar{6}$0) reflection, 3hr 45min ; Spectrograph II.

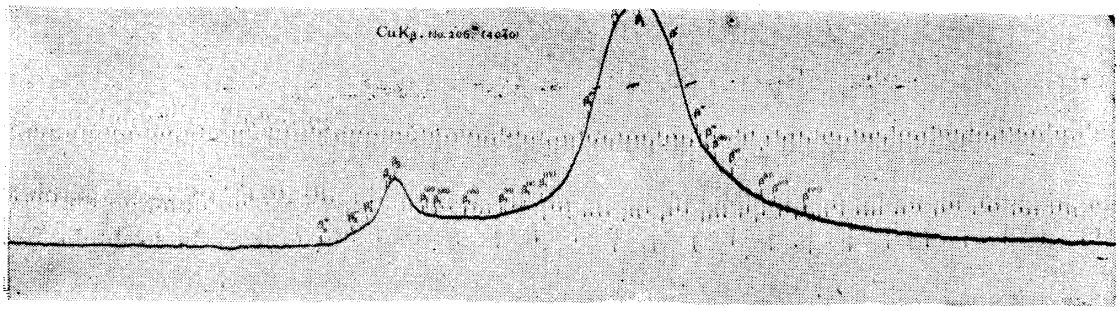

Fig. 20. The microphotometric curve of Cu$K\beta$—(40$\bar{4}$0) reflection, 17hr 15min ; Spectrograph I.

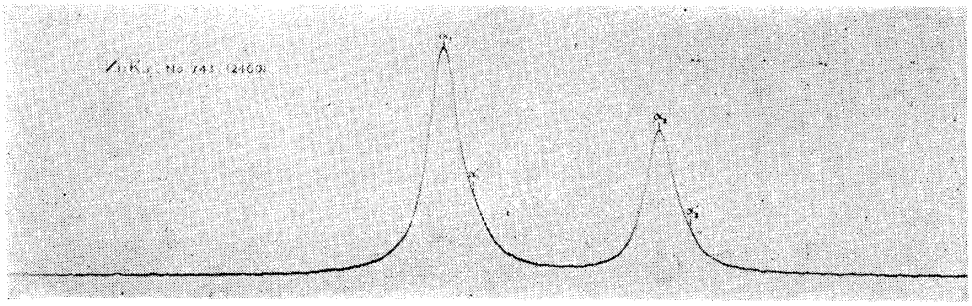

Fig. 21. The microphotometric curve of Zn$K\alpha$—(24$\bar{6}$0) reflection, 3hr ; Spectrograph II.

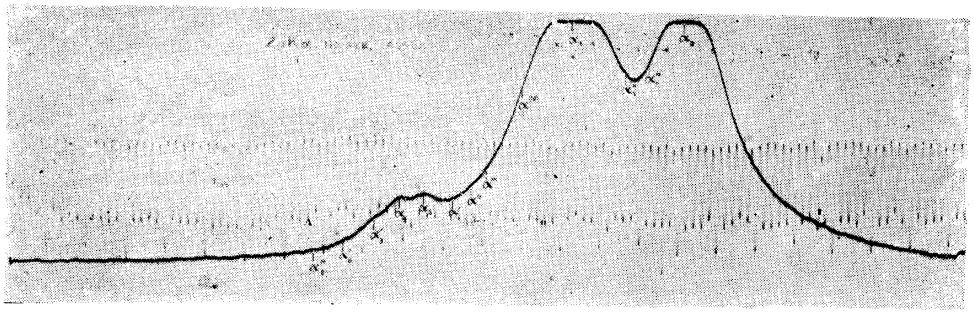

Fig. 22. The microphotometric curve of Zn$K\alpha$—(40$\bar{4}$0) reflection, 31hr 35min ; Spectrograph I.

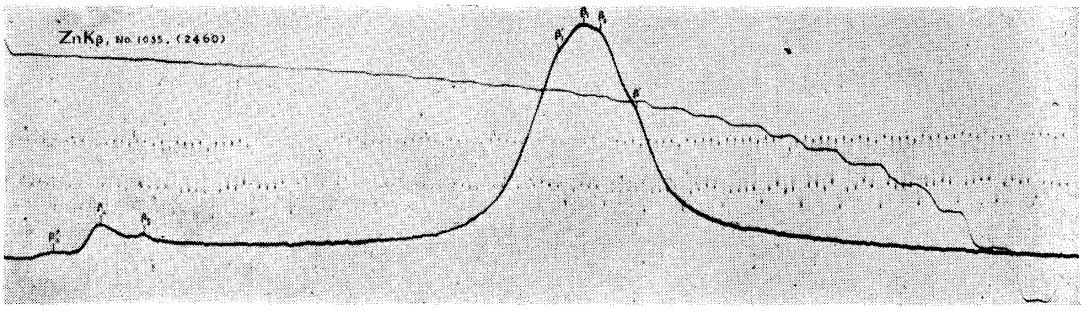

Fig. 23. The microphotometric curve of Zn$K\beta$—(24$\bar{6}$0) reflection, 39hr 30min ; Spectrograph II.

spectrograph I, having neither divided circles nor scale, so for the determination of wave-lengths, adopting three lines CuK_{α_1} ($\lambda=1537.400$ XU), ZnK_{α_1} ($\lambda=1432.22$ XU) and Cu$K_{\beta_{1,3}}$ ($\lambda=1389.35$ XU) as the reference lines, the method mentioned in II, **4**, (iii) was used. Here for the purpose of accurate measurement of distances between each two reference lines l_2—l_1 and l_3—l_1, a glass scale of 0.1 mm division was recorded on the same bromide paper with the microphotometer. The wavy curve in the figure is this, and its wave-length corresponds to 0.1 mm on the plate.

Table 3. Wave-lengths of CuK_α spectrum lines (XU).

Line symbol	$(24\bar{6}0)$ reflection	$(40\bar{4}0)$ reflection	Value given by Parratt[3]	Line symbol	$(24\bar{6}0)$ reflection	$(40\bar{4}0)$ reflection	Value given by Parratt[3]
α_0''		1528.1		$\alpha^{(VII)}$	1535.7	1535.7	
α_0'		1528.7		$\alpha^{(VIII)}$	1536.4	1536.3	
α_3'	1529.74	1529.53	1529.87	α_1	(1537.400)	(1537.400)	1537.400
α_4	1530.71	1530.60	1530.77	α_1'	1537.9	1538.0	
α_3	1531.64	1531.43	1531.57	α_1''	1539.2	1539.1	
α_3''	1532.2	1532.2		α_2	1541.23	1541.23	1541.220
α'	1533.2	1533.1	1533.01	α_2'	1541.7	1541.7	
α''	1533.5			α_2''		1543.8	
α'''	1533.9	1533.7		α_2'''		1544.2	
$\alpha^{(IV)}$	1534.1	1534.1		$\alpha_2^{(IV)}$		1545.0	
$\alpha^{(V)}$		1534.7		$\alpha_2^{(V)}$		1545.4	
$\alpha^{(VI)}$	1535.1	1535.0		$\alpha_2^{(VI)}$		1545.8	

Of the two, however, the values listed in the second column are more reliable on account of the higher degree of dispersion.

(b) CuK_β

Fig. 19 shows that which was obtained by $(24\bar{6}0)$ reflection using the spectrograph II. For the wave-length determinations, using β_1 and β_5 as the reference lines, and adopting the values given by Bearden and Shaw[2]

$$\lambda_{\beta_1}=1389.364 \text{ XU}, \qquad \lambda_{\beta_5}=1378.28 \text{ XU}$$

as their wave-lengths, the relative measurements were carried out.

In the case of a long exposure for $(40\bar{4}0)$ reflection using the spectrograph I, the microphotometric curves were obtained as shown in Fig. 20.

Investigating several such curves, still more faint lines β_2''', $\beta_1^{(IX)}$, $\beta_1^{(VIII)}$, $\beta_1^{(VII)}$, $\beta_1^{(VI)}$, $\beta_1^{(V)}$, $\beta_1^{(IV)}$, β'', β''', $\beta^{(IV)}$, $\beta^{(V)}$, $\beta^{(VI)}$, $\beta^{(VII)}$, $\beta^{(VIII)}$ are seemed to exist. The wave-lengths of these lines, as well as those obtained from Fig. 19, are

(3) L. G. Parratt, Phys. Rev. **50** (1936), 1.

Table 4. Wave-lengths of CuK_β spectrum lines (XU).

Line symbol	Obs. value	Cauchois' value	Line symbol	Obs. value	Cauchois' value
* β_2'''	1374.8		β_1'	1388.79	
β_2''	1376.26	1376.06 (β_{11}''')	β_1	(1389.364)	
β_2'	1377.01	1376.92 (β''')	β_3	1389.77	1389.74 (β_3)
β_2	1377.82		β'	1390.68	1390.73 (β')
β_5	(1378.28)	1378.68	* β''	1391.8	
* $\beta_1^{(IX)}$	1379.5		* β'''	1392.4	1392.48
* $\beta_1^{(VIII)}$	1380.1	1380.2 (β_6)	* $\beta^{(IV)}$	1392.7	
* $\beta_1^{(VII)}$	1381.4	1381.3 (β'')	* $\beta^{(V)}$	1393.7	1393.72
* $\beta_1^{(VI)}$	1383.1		* $\beta^{(VI)}$	1394.9	
* $\beta_1^{(V)}$	1383.8	1383.4 (β'')	* $\beta^{(VII)}$	1395.5	1395.6
* $\beta_1^{(IV)}$	1385.3	1384.5 (β_7)	* $\beta^{(VIII)}$	1396.8	1396.7
β_1'''	1387.34				1404.9 (β_9)
β_1''	1388.30	1388.50 (β_{10})			1405.7 (β_9)

In the table those marked with * are the lines obtained from (40$\bar{4}$0) reflection.

listed in the second column in Table 4. For the determination of wave-lengths again the lines CuK_{β_1}, ZnK_{α_1} and CuK_{α_1} are adopted as the reference lines.

Nevertheless among those obtained by (40$\bar{4}$0) reflection the lines doubtful because of their extremely weak intensities are involved, yet the coincidence with those given by Cauchois[4] are recognized on the whole.

(c) Zn K_α

Fig. 21 shows a curve of ZnK_α spectrum. Besides α_1, α_2 the weak lines α_1', α_2' are seemed to exist. As the reference lines were used α_1 and α_2, and as their wave-lengths the values given by Parratt[3] i.e.

$$\lambda_{\alpha_1}=1432.22\ \text{XU}, \qquad \lambda_{\alpha_2}=1436.05\ \text{XU}$$

were adopted.

Fig. 22 shows a curve in the case of long exposure for (40$\bar{4}$0) reflection. By comparative investigation of several such curves the weak lines α_0'', α_0', α_3', α_4, α_3, α', α'', α''', $\alpha^{(IV)}$, α_1'', α_1''' are recognized. Among these lines α_3', α_4, α_3 and α'' are well seen with the naked eye.

For the determination of wave-lengths adopting the values given by Paratt[3] as the wave-lengths of the reference lines α_4, α_1 and α_2, the method stated in II, **4**, (iii) was followed (the second column in Table 5).

(d) Zn K_β

In Fig. 23, besides β_1 and β_2, the weak lines β_2', β_5, β_1', β_3 and β' are recognized.

Adopting β_1 and β_2 as the reference lines and using the values given by

(4). Y. Cauchois, Comptes rendus, Tome 201 (1935).

Table 5. Wave-lengths of ZnK_α spectrum lines (XU).

Line symbol	Obs. value	Parratt's value	Line symbol	Obs. value	Parratt's value
* α_0''	1423.73		* $\alpha^{(IV)}$	1430.41	
* α_0'	1424.43		α_1	(1432.22)	1432.22
* α_3'	1425.14	1425.28	α_1'	1432.74	
* α_4	(1426.13)	1426.13	* α_1''	1434.02	
* α_3	1426.97	1426.98	* α_1'''	1434.88	
* α'	1427.95	1427.98	α_2	(1436.05)	1436.05
* α''	1428.56		α_2'	1436.62	
* α''	1429.20				

In the table those marked with * are the lines obtained by (40$\bar{4}$0) reflection.

Bearden and Shaw[2] as their wave-lengths, the wave-lengths of the faint lines become as listed in the next table on the assumption of linear relation between the line distance and the wave-length.

A curve obtained by (40$\bar{4}$0) reflection under long exposure is as shown in Fig. 24. Investigating several such curves, the further weak lines β_2'', $\beta_1^{(VI)}$, $\beta_1^{(V)}$, $\beta_1^{(IV)}$, β_1''', β_1'', β'', β''', $\beta^{(IV)}$, $\beta^{(V)}$ are seemed to exist.

The wave-lengths of these lines are listed in Table 6 together with those obtained above. In the table, the lines marked with * indicate those obtained by (40$\bar{4}$0) reflection, and for the determination of their wave-lengths three lines ZnK_{β_2}, Zn K_{β_1} and Cu K_{β_1} were adopted as the reference lines, using the values given by Bearden and Shaw[2] as their wave-lengths, and the method related in II, 4, (iii) was followed.

Table 6. Wave-lengths of Zn K_β spectrum lines (XU).

Line symbol	Obs. value	Value given by other obs.	Line symbol	Obs. value	Value given by other obs.
* β_2''	1278.44		β_1'	1291.99	1292.2 Bearden and Shaw (β'')
β_2'	1279.91	1279.5 Bearden and Shaw[2] (β''')	β_1	(1292.610)	1292.609 Bearden and Shaw
β_2	(1281.067)				
β_5	1282.09	1281.9 Beute(1930)	β_3	1293.00	
* $\beta_1^{(VI)}$	1283.08		β'	1293.85	1293.8 Bearden and Shaw (β')
* $\beta_1^{(V)}$	1284.52	1284.59 Kawata[5] (β'') (1928)			
			* β''	1295.07	
* $\beta_1^{(IV)}$	1287.83		* β'''	1296.68	
* β_1'''	1288.56		* $\beta^{(IV)}$	1298.10	
* β_1''	1289.50		* $\beta^{(V)}$	1299.15	

(e) Ni K_α

The curve of the spectrum raised by (23$\bar{5}$0) reflection using the spectrograph III ($2R$=150 cm) is shown in Fig. 25. The asymmetric structures of the lines

both α_1 and α_2 are well seen. Assuming that there exist additional lines in the long wave-length side of α_1 and α_2, the wave-lengths corresponding to the maxima of intensities of these lines are estimated as shown in the next table. As the wave-lengths of α_1 and α_2 the values given by Parratt[3] were used.

In Fig. 25, the places marked with the letters *a*, *b*, *c* and *d* correspond to the white lines.

Fig. 26 shows a curve of the spectrum obtained by using the spectrograph I ($2R$ = 50cm). Investigating four such curves, the wave-lengths as listed in the next table are obtained for the lines α_3', α_4, α_3, α', α'', α''', as their respective mean values. Among these lines α_3', α_4, α_3 and α''' are evidently recognized to the naked eye. For the determination of wave-lengths, using α_4 and α_1 as the reference lines, the values given by Parratt[3] were adopted as their wave-lengths, and the linear relation between the wave-length and the line distance was assumed.

Table 7. Wave-lengths of NiK_α spectrum lines (XU).

Line symbol	Obs. value	Parratt's value	Line symbol	Obs. value	Parratt's value
* α_3'	1645.94	1646.42	* α'''	1651.3	
α_4	(1647.04)	1647.04	α_1	(1654.51)	1654.51
* α_3	1647.92	1648.04	α_1'	1654.92	
α_3''		1648.80	α_2	(1658.34)	1658.34
* α'	1649.6	1649.94	α_2'	1658.73	
* α''	1650.3				

In the table those marked with * are the lines obtained from Fig. 26.

(f) Ni K_β

Fig. 27 is one of the curves obtained by $(2\bar{3}50)$ reflection using the spectrograph III. Investigating three such curves, lines are seemed to exist in the positions indicated in the figure.

For the determination of the wave-lengths, the wave-lengths of β_1 and β_5 which were given by Bearden and Shaw[2] were used, and a linear relation between the wave-length difference and the line distance was assumed.

Among the lines above-mentioned, β_3 is seen on the plate with the naked eye slightly separated from β_1. Besides, the lines $\overline{\beta}'$ and β' are also visible though very faint.

Using the spectrograph I, a spectrum obtained in the case of relatively long exposure is as shown in Fig. 28. Investigating three such curves, the further faint lines are seemed to exist at the places marked with $\beta_5^{(V)}$, $\beta_5^{(IV)}$, ... β_1'''. Among these, β_5''' and β_5'' are evidently visible with the naked eye on the plate. Moreover, two or three lines are seemed to be visible between $\beta_1^{(IV)}$ and β_1, but the confirmation of their positions is difficult.

For the determination of wave-lengths, using the lines β_1 and β_5 as the

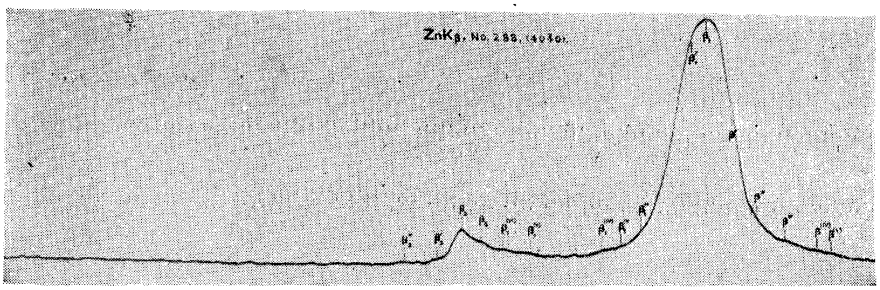

Fig. 24. The microphotometric curve of Zn $K\beta$—(4040) reflection, 31hr 35min ; Spectrograph I.

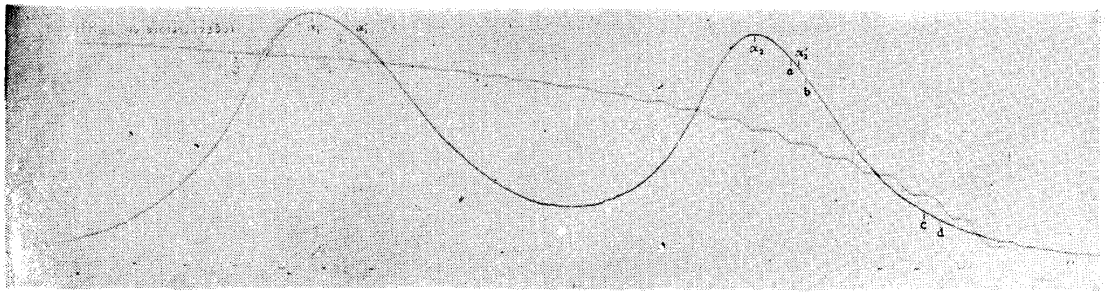

Fig. 25. The microphotometric curve of Ni$K\alpha$—(2350) reflection, 22hr 28min ; Spectrograph III.

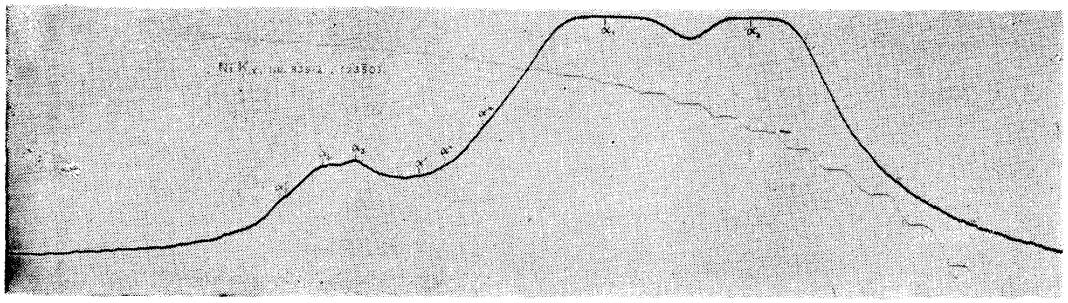

Fig. 26. The microphotometric curve of Ni$K\alpha$—(2350) reflection, 25hr 20min; Spectrograph I.

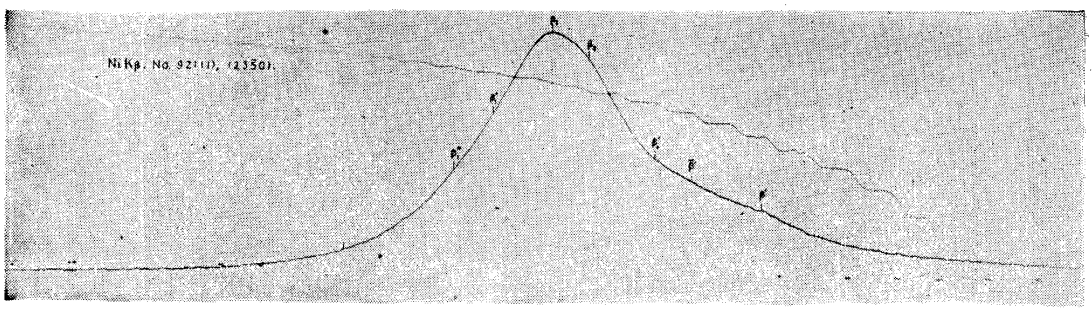

Fig. 27. The microphotometric curve of Ni$K\beta$—(2350) reflection, 46hr 42min ; Spectrograph III.

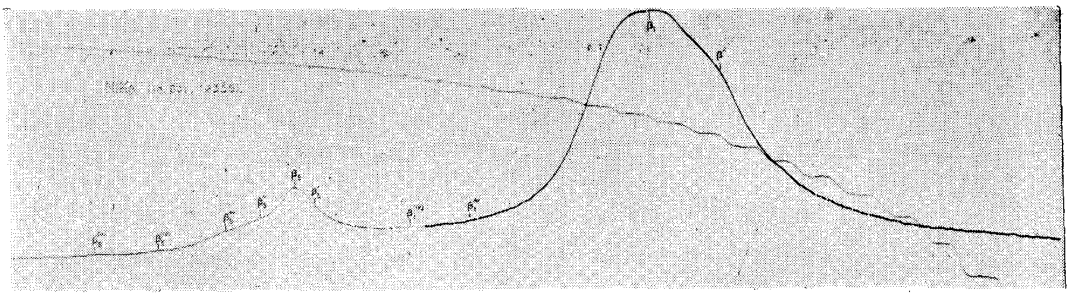

Fig. 28. The microphotometric curve of Ni$K\beta$—(23$\bar{5}$0) reflection, 23 hr ; Spectrograph I.

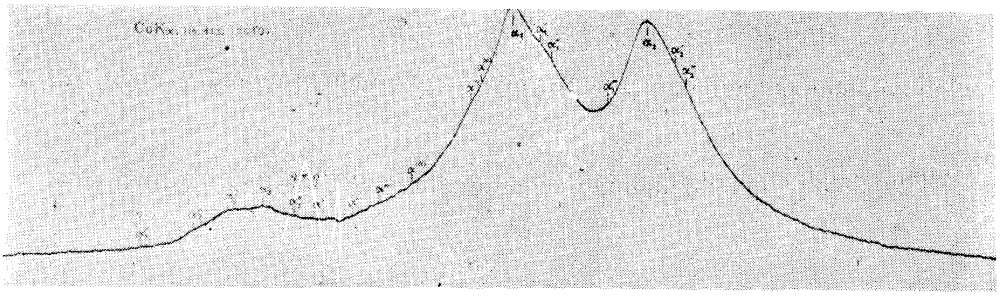

Fig. 29. The microphotometric curve of Co$K\alpha$—(40$\bar{4}$0) reflection, 38 hr 20 min ; Spectrograph I.

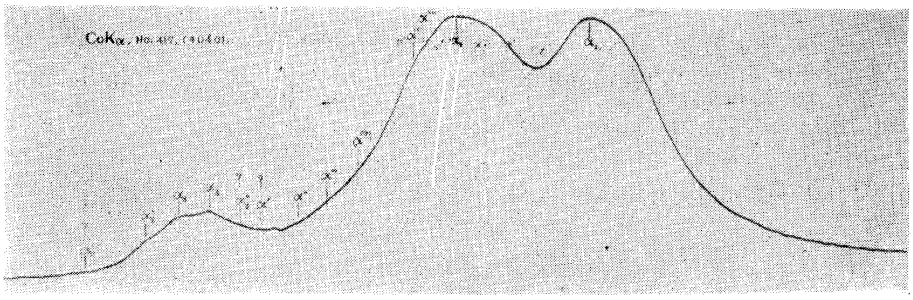

Fig. 30. The microphotometric curve of Co$K\alpha$—(40$\bar{4}$0) reflection, 100hr 10min ; Spectrograph I.

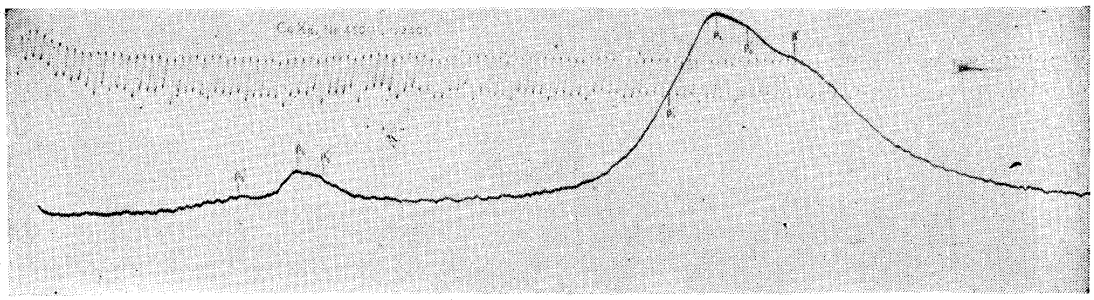

Fig. 31. The microphotometric curve of Co$K\beta$—(23$\bar{5}$0) reflection, 39 hr 55min ; Spectrograph I.

reference lines, the relation between the line intervals and wave-lengths is assumed to be linear.

Table 8. Wave-lengths of NiK_β spectrum lines (XU).

Line symbol	Obs. value	Line symbol	Obs. value	Line symbol	Obs. value
* $\beta_5^{(V)}$	1479.0	* β_5'	1486.2	β_1	(1497.080)
* $\beta_5^{(IV)}$	1481.1	* $\beta_1^{(IV)}$	1489.3	β_3	1497.49
* β_5'''	1483.28	* β_1'''	1491.2	β_0'	1498.21
* β_5''	1484.41	β_1''	1496.02	$\bar{\beta}'$	1498.60
β_5	(1485.53)	β_1'	1496.44	β'	1499.38

In the table those marked with * are the values obtained by using the spectrograph I.

(g) Co K_α

The curves obtained by relatively long exposures using the spectrograph I are shown in Figs. 29 and 30. In both curves an irregularity that appeared between α' and α'' corresponds to a white line. Investigating further seven curves like these and nine curves obtained by $(2\bar{3}\bar{5}0)$ reflection, lines are seemed to exist in the positions α_0', α_3', ..., α_2'' as indicated in the figures. Among these lines, besides α_1 and α_2, the lines α_3', α_4 and α_3 are evidently seen on the plate. α_1' and α_1'' united together to one line, are also seen distinctly separated from α_1; and $\alpha^{(V)}$ and $\alpha^{(VI)}$ are recognized, slightly separated from α_1. α''' is recognized on the plate. α_0', α_3'', α', $\alpha^{(IV)}$ and α''' are of the degree that they are seemed to be recognized on some plates though very uncertain.

For the determination of the wave-lengths, FeK_{β_1}, CoK_{α_1} and CoK_{α_2} were adopted as the reference lines, and as their wave-legnths the values given by Bearden and Shaw[3] were used.

Determining the wave-lengths by the method mentioned in II, 4, (iii), we obtained the values as shown in Table 9. Furthermore Fig. 29, from its asymmetric construction in the vicinity of the maximum value of α_1 leads us to con-

Table 9. Wave-lengths of CoK_α spectrum lines (XU).

Line symbol	Obs. value	Parratt's value	Line symbol	Obs. value	Parratt's value
α_0'	1774.4		$\alpha^{(V)}$	1784.1	
α_3'	1775.93	1776.4	$\alpha^{(V)}$	1784.35	
α_4	1777.02	1777.02	α_1	(1785.314)	1785.314
α_3	1777.96	1778.10	α_1'	1786.15	
α_3''	1778.8	1779.05	α_1''	1786.5	
α'	1779.5		α_1'''	1788.0	
α''	1780.6	1780.10 (α')	α_2	(1789.173)	1789.173
α'''	1781.45		α_2'	1790.04	
$\alpha^{(IV)}$	1782.4		α_2''	1790.3	

jecture the existence of another line between α_1 and α_1' and this view agrees with the result of the resolution of the spectrum line which will be mentioned in III, 3.

In the table, a rather large difference of the wave-length of α_3' is seen between the measured and that given by Parratt[3], because the latter is the value obtained as the result of resolution of $\alpha_{3,4}$-satellite into three component lines α_3', α_4 and α_3.

(h) Co $K\beta$

Microphotometric curves obtained are as shown in Figs. 31 and 32. On the plate corresponding to Fig. 31, β_0' and β_5' are seen separated from β_1 and β_5 respectively. β' and β_5'' are evidently recognized on the both plates, and β_5''' on the plate corresponding to Fig. 32. Moreover on this plate β'' and $\beta_5^{(IV)}$ are seemed to be recognized, though very uncertain. The wave-lengths of these lines are listed in the next table. Of these β_0' and β_1' were determined from Fig. 31, and the other lines from four curves equivalent to Fig. 32.

The wave-lengths are determined on the assumption of linear relation between the wave-length and the position of the line, adopting the values given by Bearden and Shaw[2] as the wave-lengths of the reference lines β_1 and β_5.

Table 10. Wave-lengths of Co$K\beta$ spectrum lines (XU).

Line symbol	Obs. value	Bearden and Shaw's value	Line symbol	Obs. value	Bearden and Shaw's value
$\beta_5'^{(IV)}$	1602.73		β_1'	1616.16	
β_5'''	1603.44		β_1	(1617.483)	1617.483
β_5''	1603.94	1603.8 (β''')	β_0'	1618.34	
β_5	(1605.58)	1605.58	β'	1619.66	1619.7
β_5'	1606.30		β''	1620.67	

(i) Fe $K\alpha$

A microphotometric curve obtained by $(23\bar{5}0)$ reflection using the spectrograph II is shown in Fig. 33. In the figure *a* indicates a white line.

Investigating sixteen curves similar to Fig. 33, weak lines are seemed to exist in the positions indicated with α''', α_1' and α_2'. Among these, α''' is seemed to be recognized on some plates.

Next, on the curve obtained by $(40\bar{4}0)$ reflection (see Fig. 34) the asymmetric structures of α_1 and α_2 are evidently seen and slight humps are also seen in the positions denoted by α''' and α_1'.

Fig. 35 shows the case when a long exposure was applied for the reflection $(40\bar{4}0)$.

α_3', α_4, α_3 and α'' are seen beyond doubt directly on the plate. A broad band, which will probably be composed of more than one spectrum line, is seen in

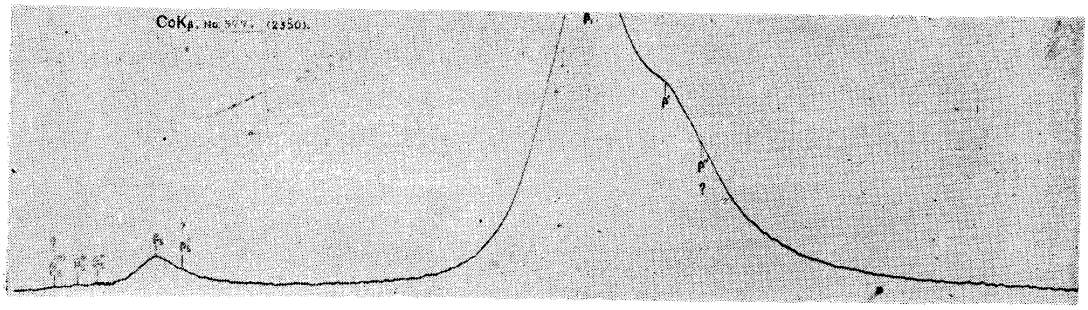

Fig . 32. The microphotometric curve of Co$K\beta$—(23$\bar{5}$0) reflection, 38hr 40min ; Spectrograph I.

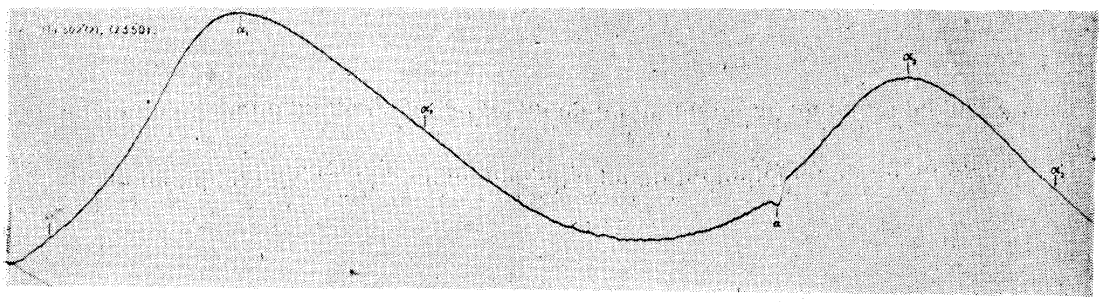

Fig. 33. The microphotometric curve of Fe$K\alpha$—(23$\bar{5}$0) reflection, 1hr ; Spectrograph II.

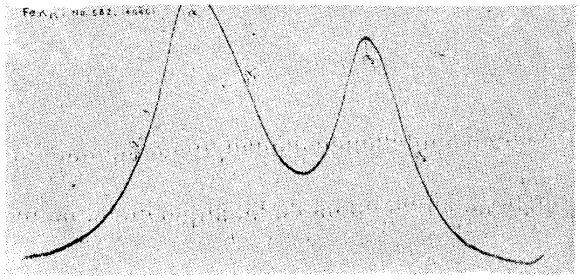

Fig. 34. The microphotometric curve of Fe$K\alpha$— (40$\bar{4}$0) reflection, 2 hr ; Spectrograph II.

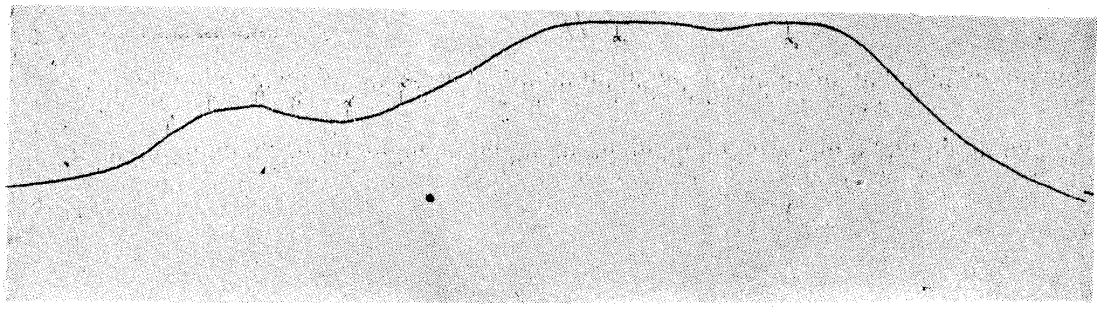

Fig. 35. The microphotometric curve of Fe$K\alpha$—(40$\bar{4}$0) reflecton, 40hr ; Spectrograph II.

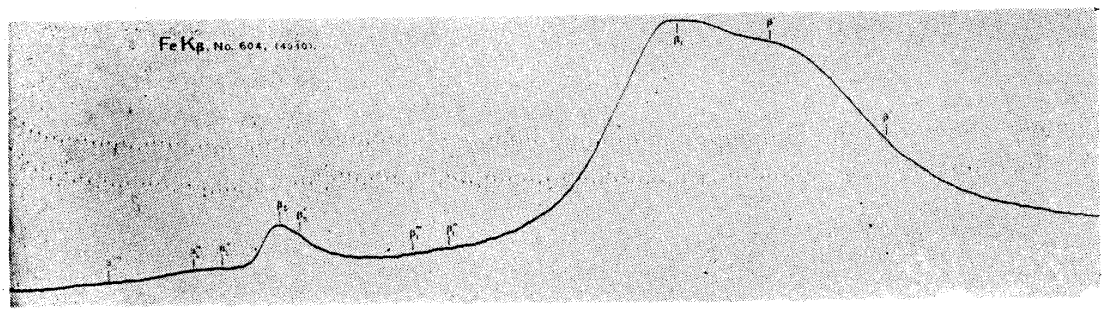

Fig. 36. The microphotometric curve of Fe$K\beta$—(4040) reflection, 57hr 30min ; Spectrograph II.

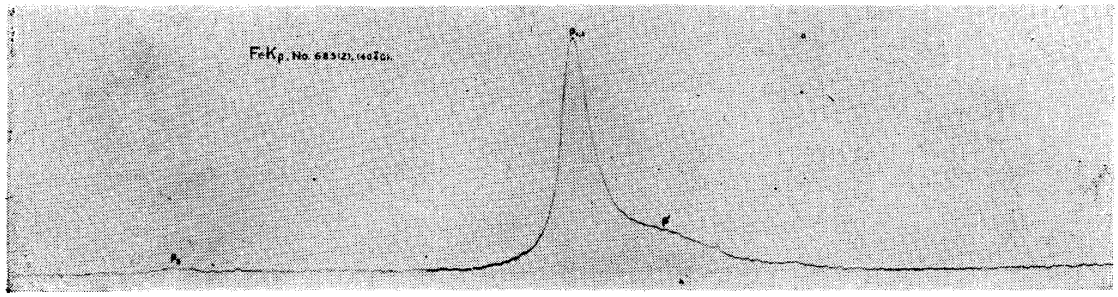

Fig. 37. The microphotometric curve of Fe$K\beta$— (4040) reflection, 1hr 20min ; Spectrograph II.

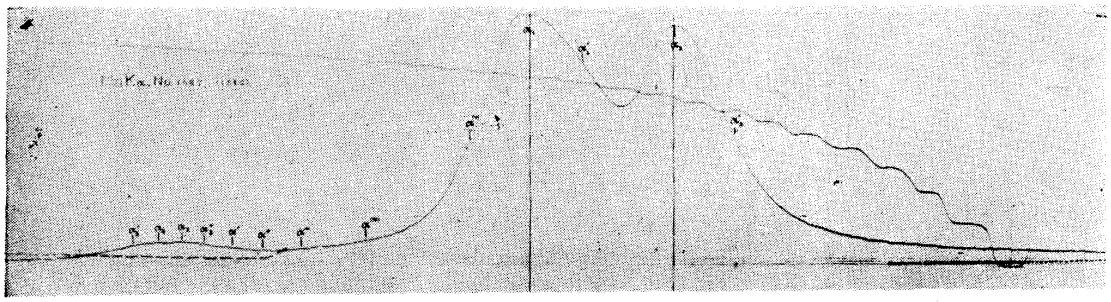

Fig. 38. The microphotometric curve of Mn$K\alpha$—(1340) reflection, 36hr 10min ; Spectrograph II.

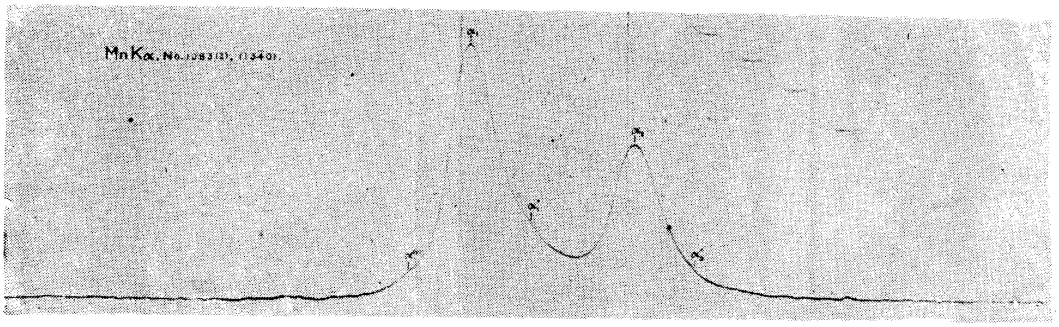

Fig. 39. The microphotometric curve of Mn$K\alpha$—(1340) reflection, 3hr 30 min ; Spectrograph II.

the vicinity of α_3''. The wave-lengths were determined as the mean values of four similar curves as the above.

For the determination of the wave-lengths in the case of $(40\bar{4}0)$ reflection, the method mentioned in II, 4, (i) was followed.

Table 11. Wave-lengths of FeK_α spectrum lines (XU)

Line symbol	Obs. value	Parratt's value[3]	Line symbol	Obs. value	Parratt's value[3]
* α_3'	1922.06	1922.16	α'''	1930.9	
* α_4	1922.69	1922.76	α_1	(1932.070)	1932.070
* α_3	1923.77	1923.94	α_1'	1933.1	
* α_3''	1924.7	1924.92	* α_2	1935.95	1936.00
* α'	1925.95	1926.05	α_2'	1936.9	
* α''	1927.2				

In the table those marked with * indicate the lines obtained from $(40\bar{4}0)$ reflection.

(j) Fe K_β

A curve obtained by applying long exposure is shown in Fig. 36.

Investigating five similar curves, besides β_5, β_1 and β', faint lines are seemed to exist in the positions indicated by $\beta_5^{(IV)}$, β_5''', β_5'', β_5', β_1''' and β_1''. Of these, β'''_5 and β_5'' are seen together as a broad line with the naked eye on many plates, but on one plate decidedly separated, and on this plate a very faint line is seen at the place regarded to correspond to β''. As for β_5', since it is not recognized with the naked eye, it is not sure. In the vicinity of the places denoted by β_1''' and β_1'' a broad line can be seen vaguely. Probably β_1''' will be Kawata's line[5] but these lines are difficult to grasp surely.

The position of β' is decided from a short exposed plate (see Fig. 37).

For the determination of the wave-lengths, using β_1 as the reference line, the method related in II, 4. (i) was followed. The results are listed in Table 12.

Table 12. Wave-lengths of FeK_β spectrum lines (XU).

Line symbol	Obs. value	Value given by others	Line symbol	Obs. value	Value given by others
$\beta_5^{(IV)}$	1735.18		β_1'''	1744.73	Kawata 1744.99
β_5'''	1737.92	Kawata 1737.97	β_1''	1745.92	
β_5''	1738.82		β_1	(1752.991)	Bearden and Shaw 1752.991
β_5	1740.62	Bearden and Shaw 1740.54	β'	1755.82	Bearden and Shaw 1756.0
β_5'	1741.26		β''	1760.27	

(5) S. Kawata, Mem. Coll. Sci. Kyoto Imp. Univ. (A) **13**(1930), 383.

(k) Mn K_α

A microphotometric curve obtained by $(1\bar{3}40)$ reflection, using the spectrograph II applying relatively long exposure, is shown in Fig. 38.

This photogram is not yet sufficient in exposure to see satellite lines, so that α_4 and α_3 can be just faintly separated to the narked eye. But $\alpha^{(V)}$ and α_1' are seen as cliffs. And there is seen a graded band in the region of $\alpha^{(IV)}$. Probably it will be composed of two or three lines. α_3'', α', α'', α''' and α_2' are not visible to the naked eye. $\alpha^{(V)}$ and α_2' are, however, rather better seen on a relatively short exposed plate as shown in Fig. 39.

Using α_1 as the reference line, the wave-lengths of all other lines were determined by the method (i) in II, 4 (Table 13).

Table 13. Wave-lengths of MnK_α spectrum lines (XU).

Line symbol	Obs. value	Parratt's value[3]	Line symbol	Obs. value	Parratt's value[3]
α_3'	2086.75	2086.55	$\alpha^{(IV)}$	2093.16	
α_4	2087.46	2086.92	$\alpha^{(V)}$	2095.97	
α_3	2088.10	2088.32	α_1	(2097.51)	2097.51
α_3''	2088.72		α_1'	2099.00	
α'	2089.50	2089.33 (α_3'')	α_2	2101.46	2101.44
α''	2090.32	2090.92 (α')	α_2'	2103.08	
α'''	2091.36				

(l) Mn K_β

Though photograms of MnK_β spectrum were taken, because of insufficient exposure, besides β_1 only β' could be recognized. One of the microphotometric curves is shown in Fig. 40.

Adopting MnK_{β_1}, FeK_{α_1} and FeK_{α_2} as the reference lines, and using the values given by Bearden and Shaw[2] as their wave-lengths, the wave-length was determined by the method mentioned in II, 4, (iii), giving the value

$$\lambda_{MnK_{\beta'}} = 1910.55 \text{ XU}.$$

(m) Ge K_α

As already stated in II, 1, (b), Ge-metal was used as emitter by rubbing onto the anticathode, and consequently very long exposure had to be applied to obtain a photogram of high degree of blackness. Even in the case when 40 hours' exposure was applied sufficient blackness was not gained to find out $\alpha_{3,4}$ satellites, so this experiment will be performed another time. But it is worth notice that the structures of α_1 and α_2 are very symmetric compared with those of the elements lower than Zn in atomic number (see Fig. 41).

(n) Ge K_β

Very long exposures are needed as in the case of GeK_α, and it could not be succeeded to obtain sufficient blackened photogram for K_β. One of the microphotometric curve is shown in Fig. 42 in which β_3 can be recognized evidently. To the naked eye, the region of β_3 is seen like an edge on the plate. β_2 is seen evidently, and β_2' and β_5 are also visilbe though faint.

Using Bearden and Shaw's values[2] for the wave-lengths of β_1 and β_2, the wave-lengths were determined on the assumption of linear relation between the wave-length and the position of the line (Table 14).

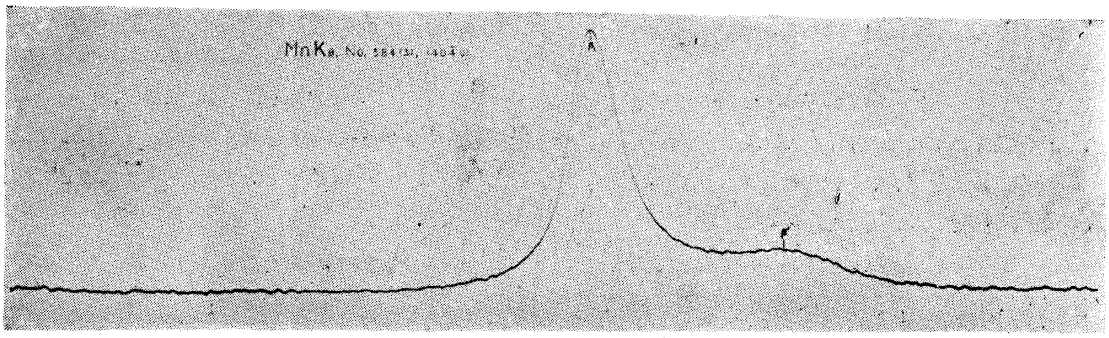

Fig. 40. The microphotometric curve of MnK_β—(40$\bar{4}$0) reflection, 7hr 20min; Spectrograph II.

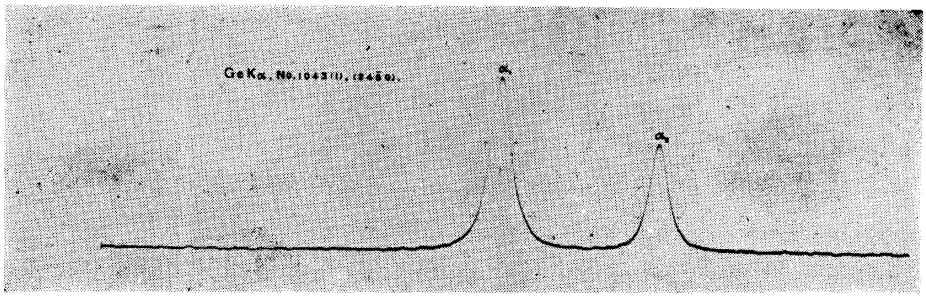

Fig. 41. The microphotometric curve of GeK_α—(24$\bar{6}$0) reflection, 2hr 30min; Spectrograph II.

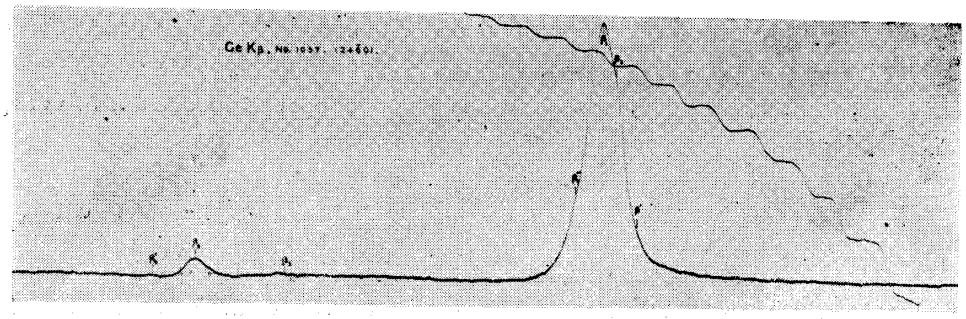

Fig. 42. The microphotometric curve of GeK_β—(24$\bar{6}$0) reflection, 44hr 15min; Spectrograph II.

Table 14. Wave-lengths of GeK_β spectrum lines (XU).

Line symbol	Obs. value	Bearden and Shaw's value	Line symbol	Obs. value	Bearden and Shaw's value
β_2'	1113.31	1113.3 (β''')	β_1	(1126.618)	1126.618
β_2	(1114.57)	1114.57	β_3	1127.01	
β_5	1117.25	1117.2	β'	1127.67	
β_1''	1125.84	1126.0 (β'')			

(o) Conclusion

In the above-mentioned experiments many faint lines were found for the elements Mn, Fe, Co, Ni, Cu, Zn and Ge. Some correlations are expected among these lines themselves and also between these lines and the fine structures of absorption spectra ; about these problems are expected the further developments. Among the above results, however, the next following points are especially noticed :

(i) The wave-length differences α_1—α_1' and α_2—α_2' are nearly equal with each other for every one of the elements stated.

(ii) The wave-length separations of Mn$K_\alpha^{(V)}$, Fe$K_{\alpha'''}$ and Co$K_\alpha^{(VI)}$ from their own K_{α_1} are nearly equal to the wave-length separations α_1—α_1' of the corresponding elements. Especially in the case of Co, furthermore, $\alpha^{(V)}$ and α_1'' are equally apart from α_1. In the case of Zn also $\alpha^{(IV)}$and α_1'' are equally apart from α_1; and such like things.

From these facts it is suggested that some certain common casues are related with the occurrence of these lines. On this problem we will return again in the last paragraph.

Similar relations occur in the β-spectra :

(iii) The separations β_5'''—β_5 of Fe, Co and Ni ; β_2'—β_5 of Cu, β_2'—β_2 of Zn are equal to their own β_1—β' separations.

These lines will also occur probably accompanied by some certain common phenomena.

Finally, the more reasonable values of the wave-lengths of the weak lines can be determined when all parts of the spectrum are expressed with actual scale of intensity and are resolved into their component lines. For this purpose, as will be mentioned in the next paragraph, the intensity measurement was performed and in the paragraph after next, the resolutions of the spectrum lines into components were tried.

2. Measurements of intensity distributions of x-ray spectra

For the intensity measurements of the x-ray spectra, the photogram-microphotometer method is considered to be inferior to the double crystal spectrometer method. The main cause for this seems to be attributable to the photographic grain effect on the microphotometric curves.

The present writer carried out the intensity measurements for K_α and K_β spectra of the elements Mn (25)—Zn (30) and Ge (32) by using bent crystal spectrographs and the auxiliary lenses[6] for a microphotometer, and obtained the results comparable in accuracy with those obtained by using double crystal spectrometers.

(a) Intensity mark

The method of rotating sector was adopted to obtain the intensity mark for the sake of simplicity of apparatus and procedure (Fig. 43).

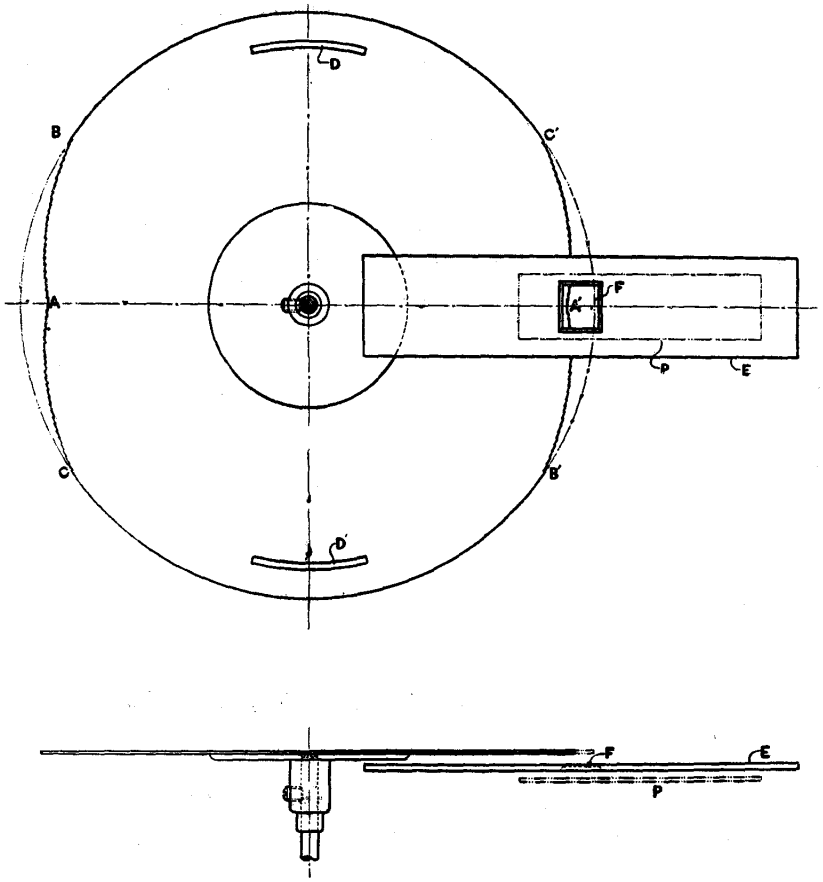

Fig. 43. A schematic diagram of the intensity mark recording apparatus.

A rotating circular plate, which has two steps-like openings BAC and B′A′C′ and two holes D and D′, is rotated in the position close to and on the same side of F, the window of a screening plate E, with the x-ray source as shown in the figure, and a photographic plate P is settled just behind E.

One of the microphotometric curves of the intensity marks is seen in Fig. 45. From such a curve, the relation between the time of exposure, and its distance from the dark line is represented in graph, then a very smooth curve as shown

(6) This paper II, 5.

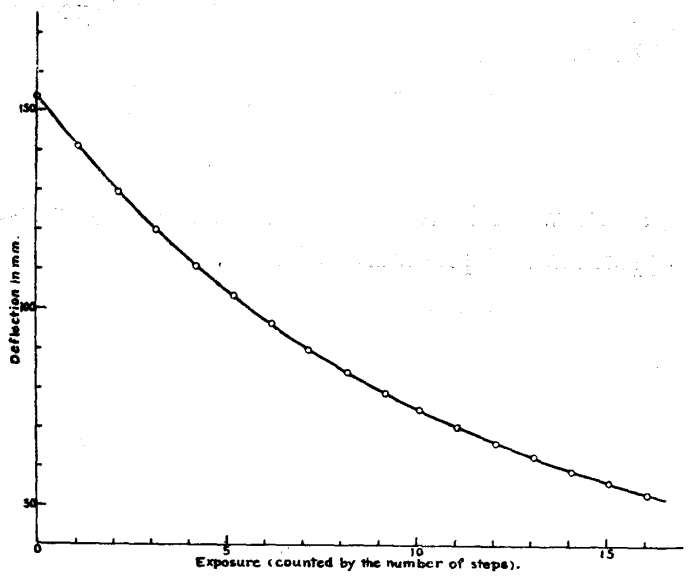

Fig. 44. Relation between the time of exposure and the deflection of the galvanometer.

in Fig. 44. is obtained.

Suppose a beam of light of the intensity J_0 fall on the plate when it is fitted on the micro-photometer, and the beam passing through it be J, then the blackness of the photogram or the photographic density S is defined by

$$S=\log_{10}J_0/J.$$

If the number of grains responsible to the absorption of the light be n, and the coefficient of absorption per grain be

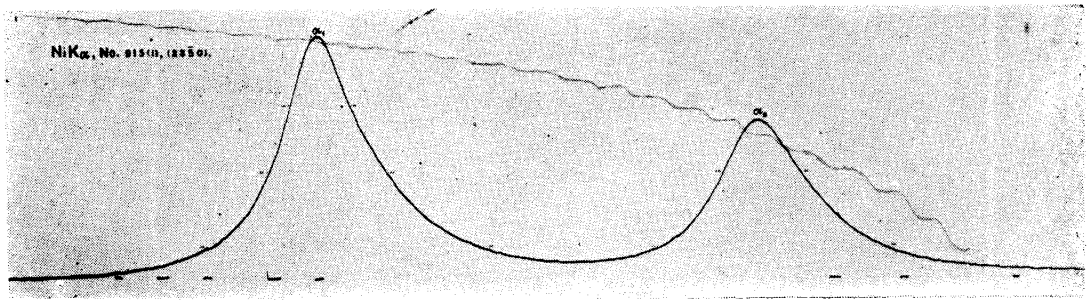

Fig. 45. Ni$K\alpha$— (23$\bar{5}$0) reflection, 4hr 5min.

K, then

$$J=J_0e^{-nK}, \qquad \therefore \quad S \propto n.$$

i.e. S denotes the number of grains and consequently the actual blakness.

Now let the intensity of radiation incident on the plate at the time of taking the photogram be I, the wave-length λ, and the time of exposure t, then S can be regarded as

$$S=f(\lambda, I, t),$$

but by Glocker and Traub's investigations[7] the form of the blackening curve is independent of λ for the range between 0.4 and 1.1 Å.

Hence S may be resolved into two factors:

$$S=g(\lambda)h(I, t).$$

(7) R. Glocker u. W. Traub, Phys. ZS. **22**(1912), 351.

In the case of visible ray, when the dependency on λ is overlooked, the consistence of the relation

$$S=H(I\cdot t^{p}) \quad \ldots\ldots\ldots\ldots\ldots (8)$$

is confirmed, p, being called Schwarzschild's exponent, is said, in the case of visible ray, to be

$$p=0.8\sim0.95$$

according to the nature of the plate.

For x-rays, we may regard to hold approximately the relation[8),(9),(10),(11)]

$$S=H(I\cdot t) \quad \ldots\ldots\ldots\ldots (9)$$

For the majority of the writer's experiments the formula (9) was used. Therefore the intensity corresponding to a certain deflection of the galvanometer is measured by the scale of time in Fig. 44. The correctness of this procedure was verified by measuring the peak ratio $K_{\alpha_1}/K_{\alpha_2}$, as it was found that almost a constant value was obtained for every one of several plates. But, on the contrary, in the case where the large value of S occurred, it was found often that the value of p in (8) was obliged to be

$$p<0.9$$

to keep that ratio at constant. Therefore it seems inadequate to regard p as constant. In such a case, the formula of the form

$$S=(I\cdot t^{1-at}) \quad \ldots\ldots\ldots\ldots (10)$$

was adopted and the value of a, a constant, was so determined that the peak ratio $K_{\alpha_1}/K_{\alpha_2}$ becomes constant for all of the photograms of various blackness, then a better coincidence with experiment could be brought.

(b) The intensity distribution curve

Some examples of the curves used for measuring the intensity distributions are shown in Figs. 45, 46, 47, and 48. The intensity distribution is obtained as the average of the intensity distributions which are separately derived from several such curves. An example of the degree of agreement of three derived curves is shown in Fig. 49.

The final curves for K_α's as the averages of several curves are the outer curves denoted by $\boldsymbol{a}$'s in Figs. 50 to 56, where the small circles on the curve indicate

(8) H. Kröncke, Diss. Göttingen, 1913 ; Ann. d Phys. **43**(1914), 687.

(9) W. Busse, ZS. f. Phys. **34**(1925), 11.

(10) A. Bouwers, Diss. Utrecht, 1924.

(11) Jönsson, Ark. f. Mat., Astr. och. Fys. **18**(1924).

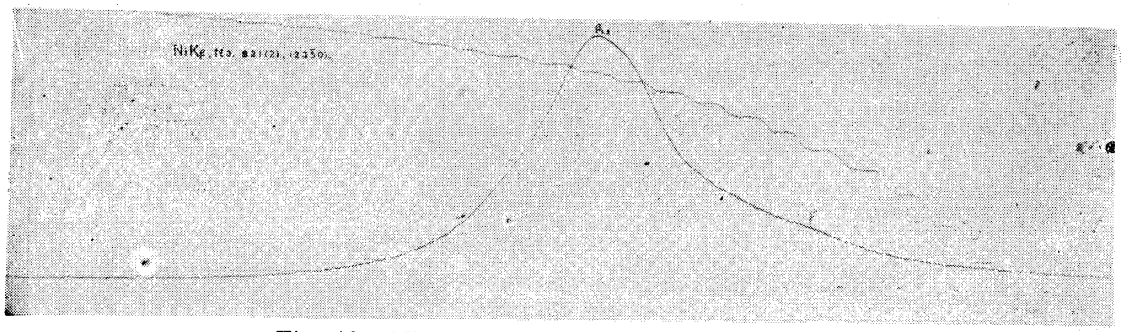

Fig. 46. Ni$K\beta$—(23$\bar{5}$0) reflection, 43hr 20min.

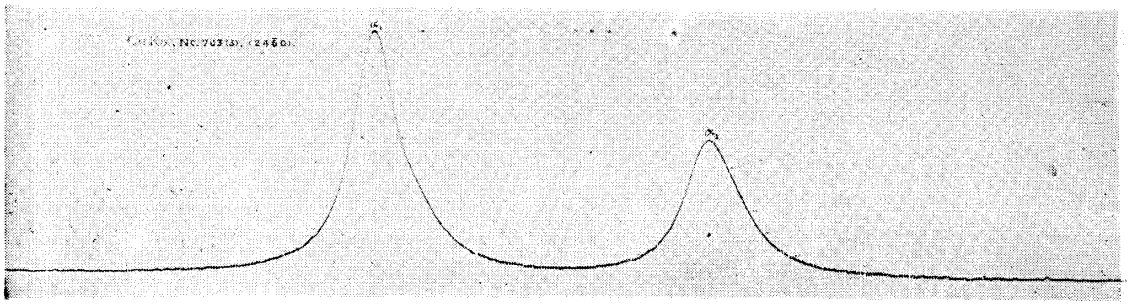

Fig. 47. Cu$K\alpha$—(24$\bar{6}$0) reflection, 30min.

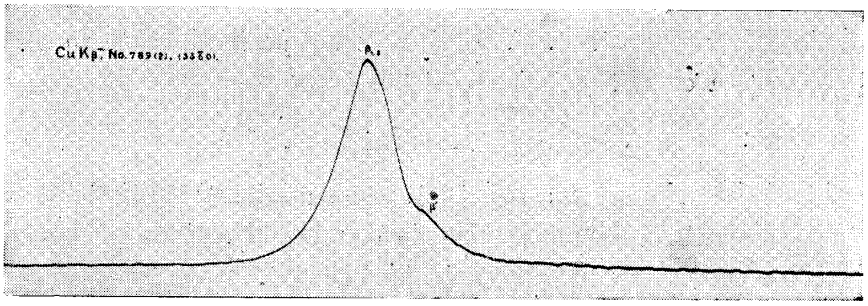

Fig. 48. Cu$K\beta$—(33$\bar{6}$0) reflection, 8hr.

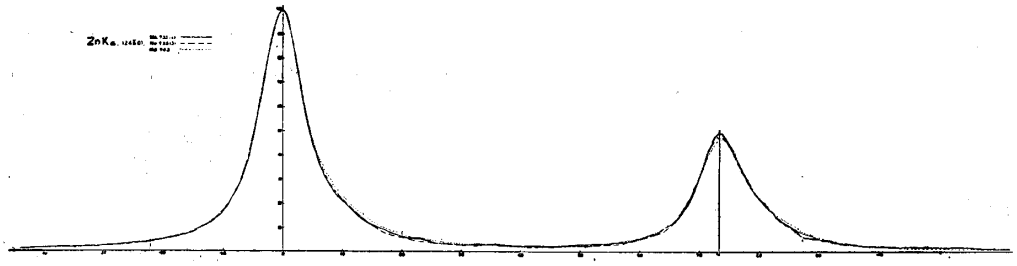

Fig. 49. Intensity distribution curves of Zn$K\alpha$—(24$\bar{6}$0) reflection, showing the degree of agreement of three curves.

the averaged values faithfully.

Similar curves for $K\beta$'s are the outer ones denoted by ***b***'s in Fig. 61 (Mn$K\beta$) and Figs. 67 (Fe$K\beta$) to 72 (Ge$K\beta$).

(c) The width at half maximum and the index of asymmetry.

The widths at half maximum and the indices of asymmetry obtained from the averaged intensity distribution curves, above mentioned, are listed in the next table.

Table 15. Widths at half maximum and indices of asymmetry.

		Width at half max. (XU)			Index of asymmetry		
		Obs. value	Parratt's value[8]	Roseberry-Bearden's value[12]	Obs. value	Parratt's value[8]	Bearden-Shaw's value[2]
$K\alpha_1$	Mn	1.10 (1.075)	1.06 (0.89)	1.05	1.36 (1.34)	1.45 (1.43)	1.41—1.52
	Fe	0.79	0.946 (0.79)	0.95	1.63	1.61 (1.60)	1.54—1.66
	Co	0.74 (0.732)	0.760 (0.63)		1.45 (1.45)	1.44 (1.44)	1.28—1.40
	Ni	0.535	0.622 (0.504)		1.25	1.22 (1.22)	1.12—1.22
	Cu	0.486	0.565 (0.460)		1.11	1.15 (1.15)	1.11—1.15
	Zn	0.481 (0.481)	0.530 (0.434)	0.527	1.07 (1.07)	1.11 (1.11)	1.06—1.12
	Ge	0.443	0.457 (0.379)		1.00	1.04 (1.04)	1.03—1.06
$K\alpha_2$	Mn	1.27 (1.24)	1.24 (1.00)	1.23	1.225 (1.24)	1.19 (1.27)	1.13—1.24
	Fe	0.982	1.10 (0.97)	1.11	1.28	1.30 (1.35)	1.22—1.30
	Co	0.974	0.97 (0.82)		1.28	1.27 (1.30)	1.25—1.30
	Ni	0.771	0.85 (0.72)		1.24	1.23 (1.25)	1.18—1.21
	Cu	0.702	0.740 (0.635)		1.28	1.28 (1.28)	1.20—1.31
	Zn	0.558 (0.543)	0.606 (0.510)	0.615	1.25 (1.26)	1.33 (1.33)	1.19—1.34
	Ge	0.475	0.482 (0.404)		1.00	1.11 (1.11)	1.08—1.11
$K\beta_{1,3}$	Mn	1.063		1.07	1.54		1.36—1.42
	Fe	1.013		1.03	1.65		1.64—1.81
	Co	1.034			1.52		1.67—1.78
	Ni	1.057			1.29		1.23—1.32
	Cu	1.013			1.09		1.09—1.19
	Zn	0.910		0.911	1.39		1.43—1.67
	Ge	0.824			1.52		1.96—2.09

In the table the parenthesized values in the column "Obs. value" are the corrected values by taking the overlapping of α_1 and α_2 into consideration. The parenthesized values in the column "Parratt's value" are the corrected values by taking the increase of width caused by the overlapping of α_1 and α_2 and by the finite resolving power of the crystal into account.

The present observed values, being compared with the values obtained by the double crystal spectrometer, are always narrower than the latter in the width at half-maximum, and lie between the values measured with the double crystal spectrometer and their corrected, with the exception of Mn, for which the values for K_{α_1} and K_{α_2} are slightly larger, this seems to be caused by the oxidation of Mn.[12]

(12) H. H. Roseberry and J.A. Bearden, Phys. Rev. **50** (1936), 204.

The circumstances are similar with regard to the indices of asymmetry. The disagreement for Ge seems to be attributed partly to the increase of errors on account of the narrow width of the spectrum line, yet leaves something to be corrected which may be caused by the aberration of the bent crystal. The slight disagreement for CoK_β seems also to be interpreted in like manner. Further experiment with the large sized spectrograph, III, will answer these subjects.

(d) The ratio of peak intensities.

The ratios of the peak intensities, i. e. the ratios of the maximum values of α_1 to those of α_2 of the corresponding elements, obtained from the curves above stated, are as listed in Table. 16. In the table the figures in the parentheses are the corrected values taking the overlapping of α_1 and α_2 into account.

Table 16. Ratio of peak intensities α_1 α_2.

Element	Obs. value	Roseberry and Bearden's value[12]	Parratt's value[13]
Mn	2.05	2.20—2.16	2.15 (2.24)
Fe	2.36	2.07	2.07 (2.16)
Co	2.425		
Ni	2.34		2.30 (2.35)
Cu	2.25		
Zn	2.08	1.99	
Ge	2.205		

(e) The overlapping factor.

The definition of the overlapping factor f_{over} is[13] :

$$f_{over} = \frac{\text{minimum ordinate between } \alpha_1 \text{ and } \alpha_2}{\text{maximum value of } \alpha_1} \times \text{ratio of intensities } \alpha_1 \text{ to } \alpha_2.$$

Table 17. Overlapping factors.

Element	Obs. value	Parratt's value[3]
Mn	0.228	0.23
Fe	0.104	0.174
Co	0.112	0.116
Ni	0.064	0.093
Cu	0.041	0.057
Zn	0.044	0.037
Ge	0.024	0.030

The values obtained from the foregoing intensity distribution curves are listed in Table 17.

The present observed values are always smaller than those obtained by a double crystal spectrometer with the exception of Zn. The reason for this may be partly due to uncertainty of the base line, mainly, however, seems to be attributable to the use of the reflection of high

(13) L.G. Parratt, Phys. Rev. **44** (1933), 695.

dispersion and to the high degree of perfection of the quartz crystal. Somewhat larger value for Zn will probably be caused by that the base line on the long wave-length side of α_2 has been drawn too low, as seen in Fig. 55. The more accurate comparison can be made readily by investigating the long exposed photogram.

(f) Conclusion.

Though the accuracy of the intensity measurement by a photogram-microphotometer method had been considered to be very inferior to the double crystal spectrometer method, now, the accuracy could be raised to the level comparable with that of the double crystal method by utilizing the reflection which gives large dispersion by the use of the bent crystal spectrograph in one hand and by using the auxiliary lenses for microphotometer in the other ; this seems to be worthy of attension with the fact indicating the high degree of perfection of the quartz crystal. The more accurate intensity measurement will possibly be carried out by taking care for the reduction of the aberration of the bent crystal.

3. Resolution of $K_{\alpha_{1,2}}$- and $K_{\beta_{1,3}}$-doublets into their component lines and correlation of the structrues of these doublets

By resolving K_{α_1} and K_{α_2} into their component lines on the assumption that either of them is composed of a principal symmetric part, which obeys to the classical dispersion formula, and a rest asymmetric part, it was shown that the asymmetric parts thus obtained resemble each other in shape. Next, by resolving $K_{\beta_{1,3}}$ doublet into component lines on the assumptions that it is composed of two principal parts β_1 and β_3, and the weaker components β', β_1', ..., each obeying the classical dispersion formula, that the ratio of total intensities $\beta_1 : \beta_3 = 2 : 1$, and that the separation β_3—β_1 agrees with "the spin-doublet formula", it was found that a component line, which bears a close resemblance in shape to the asymmetric part of α_1 or α_2 and does not belong to the component lines above denoted, can be considered to be involved. Therefore the asymmetric structures of α_1 and α_2 are understood to have correlation with each other and also with the structure of $\beta_{1,3}$.

(a) Resolution of K_{α_1}- and K_{α_2} - curves into symmetric and asymmetric component curves

Though K_{α_1}- and K_{α_2}-curves exhibit remarkable asymmetric structures especially for the elements Ti(22) — Zn(30), it has been pointed out[3] that the curves for these elements also have the shape resembling closely to that of the classical dispersion formula on the short wave-length side of α_1.

According to Williams[14], UL_{α_1} is of almost perfectly classical dispersion shape.

A. Hoyt[15] also has shown that MoK_{α_1} and WK_{α_1} are represented very accurately by the formula of the classical dispersion shape :

$$y = \frac{A}{1 + \left(\frac{x - x_0}{w}\right)^2}, \quad \cdots\cdots\cdots\cdots (11)$$

where A, w and x_0 are constants. Moreover, it is reported that the L-series lines having nearly equal wave-lengths as that of Cu K_α do not show asymmetric structures.[16] And the degree of asymmetry has been ascertained to depend on the sort of chemical combination[12][17]. These facts suggest that the outer states of atoms are concerned with the asymmetric structures.

In these circumstances it can be regarded that, although the K_α lines of the elements above mentioned are also originally to be emitted as a symmetric and classical dispersion shape, by accompanying some certain phenomena which cause changes in the outer states of atoms, the wave-lengths of the radiation concerning the phenomena are modified and then the asymmetric part is produced. On this assumption let us decompose the lines K_{α_1} and K_{α_2} into the components: the classical dispersion shaped ones and the rests. The procedure is as follows : First a formula of the classical dispersion shape is so determined that it agrees with experiment on the short wave-length side of K_{α_1} as well as possible. For this purpose in many cases the maximum value of the formula was obliged to be adopted smaller than the observed maximum, and the maximum ordinate to be shifted towards the shorter wave-length side than that of the observed. Just the same procedure is applied to α_2 . But also the overlapping of α_1 and α_2 must be taken into consideration.

As the results of the measurements mentioned in 2, this chapter agreed fairly well with that obtained by double crystal spectrometers, the resolution into component lines on the basis of the measurements were performed by following the idea above stated ; the results are shown in Fig. 50 (MnK_α)~Fig. 56 (GeK_α). In the figure $\boldsymbol{a}$ denotes the curve obtained by measurements, $\boldsymbol{a}_1$ and $\boldsymbol{a}_2$ the symmetric parts of α_1 and α_2 respectively ; and $\bar{\boldsymbol{a}}_1$ and $\bar{\boldsymbol{a}}_2$ the asymmetric parts, the rest parts which are left by subtracting $\boldsymbol{a}_1$ and $\boldsymbol{a}_2$ from $\boldsymbol{a}$ (in the case of GeK_α, however, the line widths seem to be slightly broaden on account of the aberration of the bent crystal, so $\bar{\boldsymbol{a}}_1$ and $\bar{\boldsymbol{a}}_2$ are obtained by subtracting from $\boldsymbol{a}$ the values taken symmetrical with the short wave-length sides with respect to the

(14). A. H. Compton and S. K. Allison, X-Rays in Theory and Experiment, p. 748 and references.
(15). A. Hoyt, Phys. Rev. **40** (1932), 477.
(16). A. H. Compton and S.K. Allison, X-Rays in Theory and Experiment, p. 749.
(17) L.Obert and J. A. Bearden, Phys. Rev. **54** (1938), 1000.

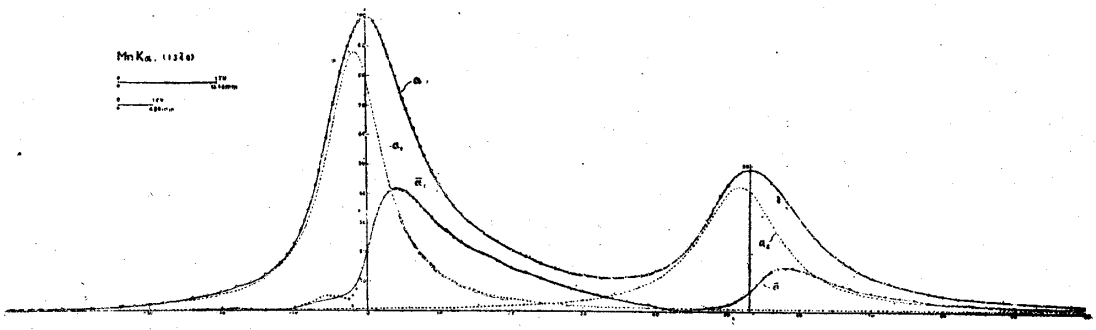

Fig. 50. The intensity distribution curve of Mn$K\alpha$ and the resolved component lines—(13$\bar{4}$0) reflection.

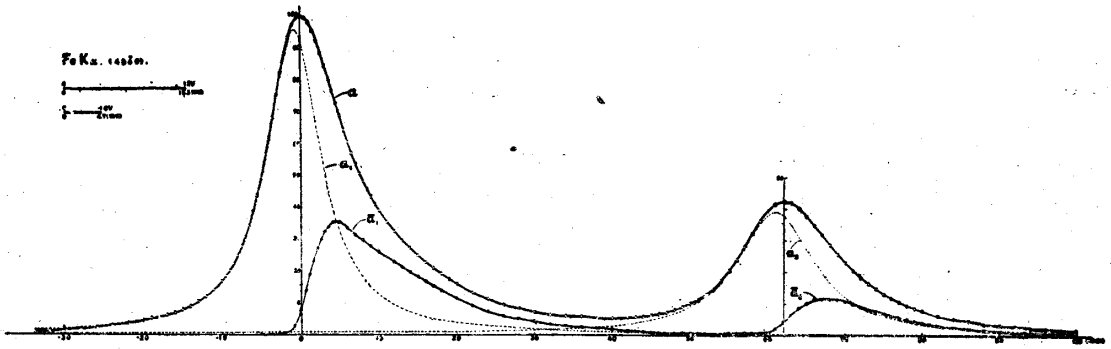

Fig. 51. The intensity distribution curve of Fe$K\alpha$ and the resolved component lines—(40$\bar{4}$0) reflection.

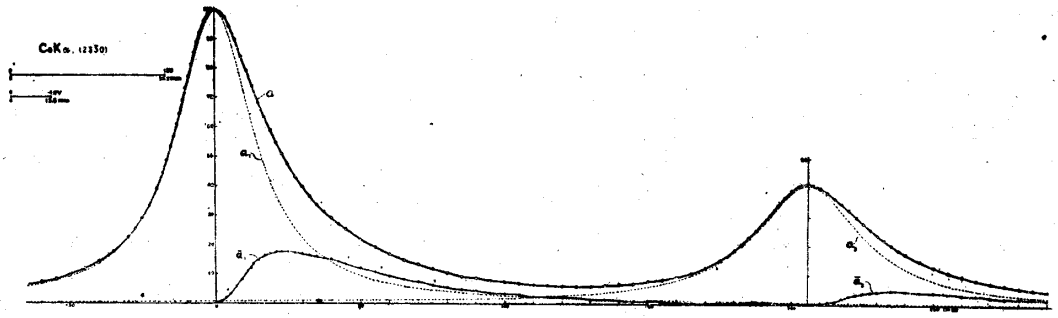

Fig. 52. The intensity distribution curve of Co$K\alpha$ and the resolved component lines—(23$\bar{5}$0) reflection.

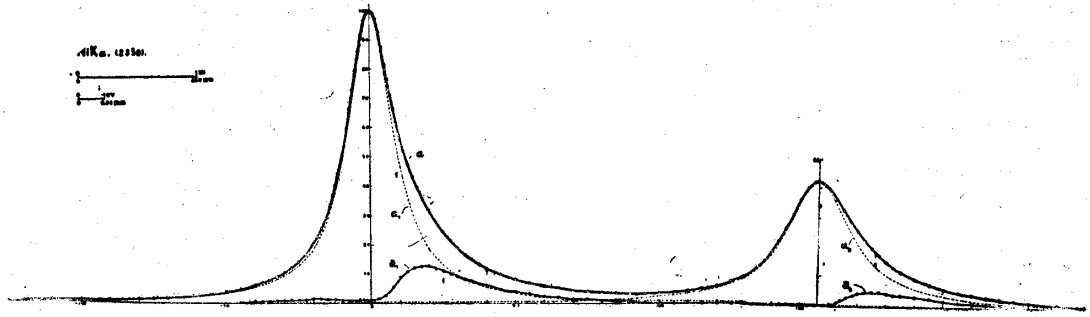

Fig. 53. The intensity distribution curve of Ni$K\alpha$ and the resolved component lines—(23$\bar{5}$0) reflection.

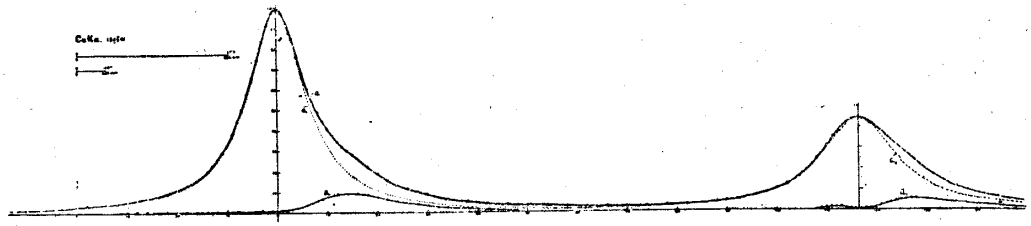

Fig. 54. The intensity distribution curve of CuK_α and the resolved component lines—(24$\bar{6}$0) reflection.

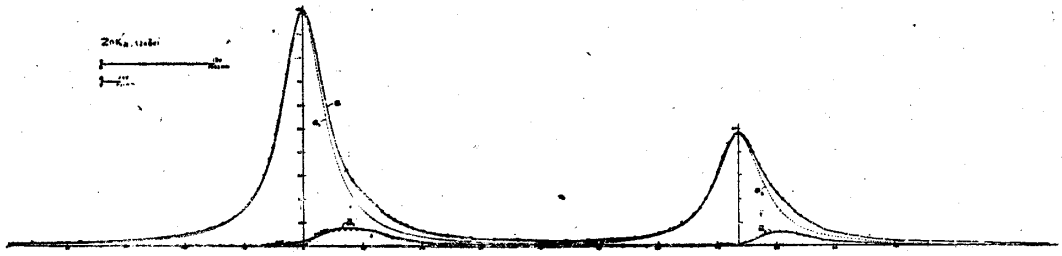

Fig. 55. The intensity distribution curve of ZnK_α and the resolved component lines —(24$\bar{6}$0) reflection.

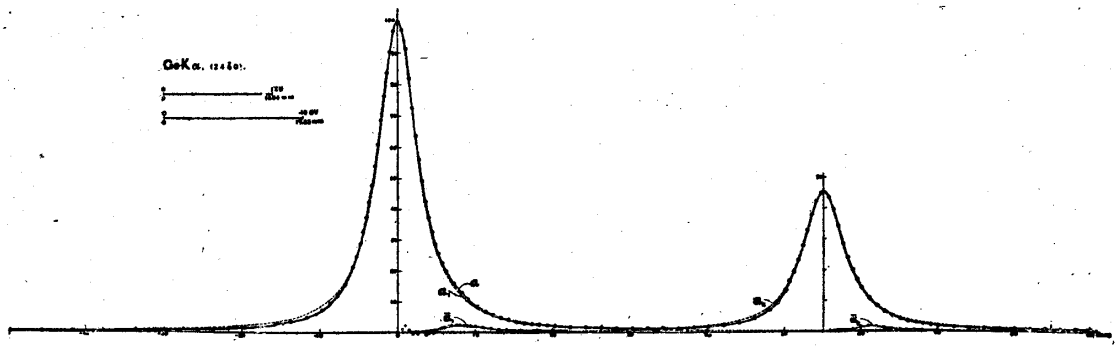

Fig. 56. The intensity distribution curve of GeK_α and the resolved component lines—(24$\bar{6}$0) reflection.

maximum ordinates). This method of resolution means that, though the lines originally to be emitted have the shapes similar to $\boldsymbol{a}_1$ and $\boldsymbol{a}_2$ in the figure, as the results of accompanying some certain changes in the outer shells of atoms, the wave-lengths of the radiation concerned with the changes are modified, producing the asymmetric parts $\overline{\boldsymbol{a}_1}$ and $\overline{\boldsymbol{a}_2}$.

The numerical vaules of the constants in Eq. (11) representing the resolved symmetrical part are listed in Table 18. In the table A_1 and A_2 indicate the maximum values for α_1 and α_2 respectively ; w_1 and w_2 the half widths at half maxima ; x_1 and x_2 the abscissae corresponding to the maximum ordinates referred to the abscissae of the maximum ordinates of α_1 and α_2 on the measured curve as the origins.

Table 18. Values of the constants for the symmetric parts.

		Mn	Fe	Co	Ni	Cu	Zn	Ge
$K\alpha_1$	A_1	90	95.5	99.5	99.7	98.5	99	99.85
	w_1(mm)	4.8	4.2	16.0	9.65	7.0	4.3	3.0
	x_1(mm)	—1.6	—0.8	0	0	0	—0.05	0
$K\alpha_2$	A_2	43	39	40.65	42.4	43.5	47.5	45.06
	w_2(mm)	6.8	6.0	22.4	13.9	8.3	4.7	3.3
	x_2(mm)	51.6	61.0	205.7	156.1	115.5	73.6	55.11
		(53.05)	(62.1)	(205.7)	(156.1)	(115.6)	(73.6)	(55.11)

In the table, the figures in the parentheses indicate $\alpha_1-\alpha_2$ separations.

(b) Resolution of $K_{\beta_{1,3}}$-doublet into component lines.

The resolution of $K_{\beta_{1,3}}$-doublet line into component lines for the elements not far from Fe in atomic number had not yet been carried out, so at first some experimental efforts were made to separate it into two component lines β_1 and β_3, as it seemed to be merely the question of the dispersion of the spectrograph.

For instance, in the case of a bent crystal spectrograph with quartz plate, for the β_1—β_3 separation of CoK_β, $(33\bar{6}0)$ reflection stands under the most favorable condition, and this separation amounts to 2°29′30″. This value corresponds about twenty-two times of the angular separation of 6.8′ which is raised by the reflection of the first order using a calcite, so that even with a bent crystal spectrograph having the focusing circle of 50 cm in diameter, the β_1—β_3 separation amounting to 21.9 mm is obtained, therefore it seemed to be able to separate $\beta_{1,3}$ into two lines β_1 and β_3. The result of experiment showed, however, merely the broadening of the whole spectrum, ending in failure.

The above result suggests that the fact that the separations of the $K_{\beta_{1,3}}$ doublets of these elements have not been carried out is not attributable to the poor dispersion, but is originated in that these two lines stand too close to each other to be separated spectro-photographically. Efforts were made to find out a method of separation of such a double line. At first, by investigating the curve form on the short wave-length side of Mn$K_{\beta_{1,3}}$, it was confirmed that it resembles to the classical dispersion formula for the most part. And as the long wave-length side of β' is also seemed to be the classical dispersion shape, so as the first approximation, on the assumption that these two lines have the shapes symmetrical with respect to their own maximum ordinates, those symmetrical values were subtracted from the original curve, taking into account the overlapping of the feet of β_1 and β'. In Fig. 57, ***b*** indicates the curve obtained by measurement. The rest part obtained by subtracting β_1 and β' from ***b*** is denoted by $\bar{\boldsymbol{b}}$ which is naturally regarded to be β_3. But $\bar{\boldsymbol{b}}$ is entirely different from the classical dispersion shape. It is hardly conceivable that β_3 alone takes such a

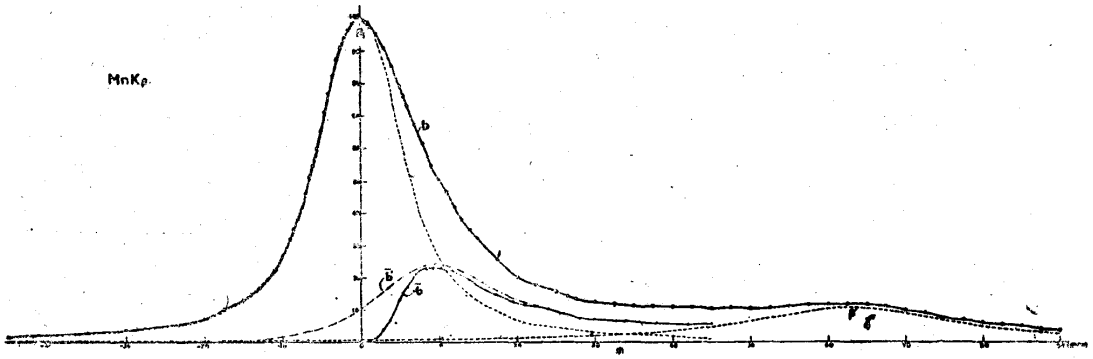

Fig. 57. Mn$K\beta$, the long wave-length side of β_1 is assumed to be symmetrical with the short wave-length side of it.

peculiar form. A method is desired which makes β_3 into a similar form. If, by scraping the head of β_1 and adding it to $\overline{b}$, it is able to convert $\overline{b}$ into the form like $\overline{b}'$, it may be possible to make $\overline{b}'$ resemble to the shape represented by Eq. (11). Accordingly, graphs are drawn for trial for the values $B_1=90$ and 80, as the height of β_1, adopting the value $w_1=6.0$ mm, which corresponds to the value of w in Eq. (11), and leaving β' as it is. Then there appears a hump on the short wave-length side of $\overline{b}$ as shown in Figs. 58 and 59, becoming a form very different from that of Eq. (11), contrary to the expectation. This hump

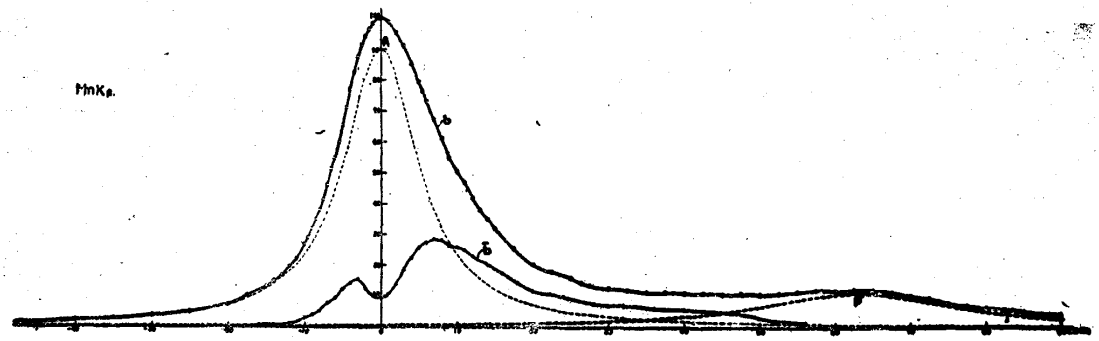

Fig. 58. Mn$K\beta$, the values $B_1=90$, $w_1=6.0$ mm $x_1=0$ are adopted.

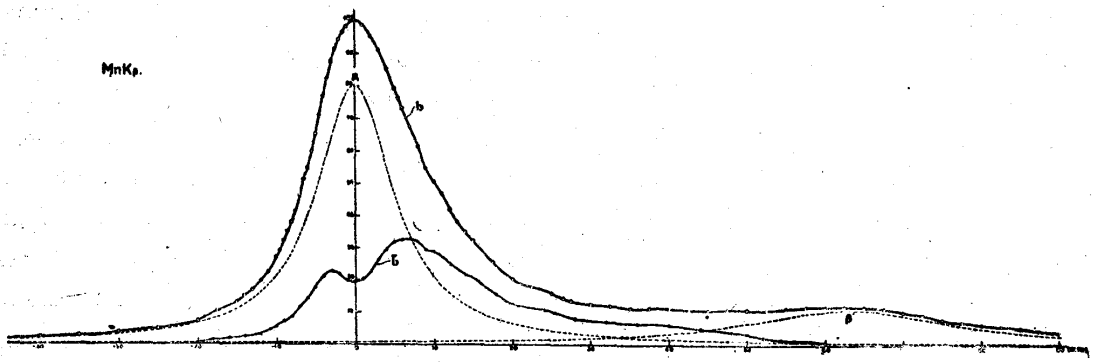

Fig. 59. Mn$K\beta$, the values $B_1=80$, $w_1=6.0$ mm, $x_1=0$ are adopted.

should be taken off, and there is a possibility of achieving this purpose by shifting the maximum ordinate of β_1 towards the short wave-length side. But it is easily conceivable that it is practically impossible to bring the whole shape of $\bar{\bar{\boldsymbol{b}}}$ in coincidence with that of Eq. (11). Therefore, the attempt to make the whole shape of $\bar{\boldsymbol{b}}$ agree with that of Eq. (11) was given up, and the resolutions were tried under the following three assumptions.

(i) The foot of $\bar{\boldsymbol{b}}$ on the short wave-length side is assumed to be of the shape of Eq. (11).

This assumption is deduced from the fact that the original curve $\boldsymbol{b}$ resembles to that of Eq. (11) in shape on the short wave-length side, consequently it may be considered to be composed of lines each having a form similar to that equation. It would be very interest, if the resolution was effected with this assumption alone and the ratio of intensities $\beta_1 : \beta_3$ and the separation β_1—β_3 were obtained, but it was found very difficult to arrive at a definite solution because of the vague nature of the problem with this assumption alone. Accordingly the next two plausible assumptions are added :

(ii) The ratio of intensities (the ratio of areas) to be $\beta_1/\beta_3=2$;

(iii) The separation (the separation in wave-length) β_1—β_3 to obey the approximate formula for a spin doublet[18]

$$\frac{\Delta\nu}{R} \propto (Z-\sigma_2)^4$$

or expressed in wave-length

$$\Delta\lambda \propto \lambda^2 (Z-\sigma_2)^4 \quad \cdots\cdots\cdots\cdots\cdots\cdots \quad (12)$$

where $\Delta\nu$ denotes the separation in wave number of β_1 and β_3, R the Rydberg constant, Z the atomic number, λ the wave-length, $\Delta\lambda$ the separation in wave-length of β_1 and β_3, and σ_2, called a screening constant, is said to have the value

$$\sigma_2=8.5 \text{ [19]}$$

in this case.

The assumption (ii) is recognized theoretically[20], and the result of measurement by Allison and Armstrong[21] for Mo(42) gives

$$K_{\beta_1} : K_{\beta_3}=2 : 1.$$

By W. H. Kliever[22]

$$\text{for W(74)}, \quad K_{\beta_1} : K_{\beta_3} = 18.1 : 9.6,$$
$$\text{for Pt(78)}, \quad K_{\beta_1} : K_{\beta_3} = 20.0 : 10.2,$$

(18) A. H. Compton and S. K. Allision, X-Rays in Theory and Experiment, p. 609.
(19) Ebenda, p. 612.
(20) Ebenda, p. 650.
(21) S. K. Allison and A. H. Armstrong, Phys. Rev. **26** (1925), 701, 714, ; (19), p. 638.

therefore 2 : 1 approximately. Though it is questionable to some extent whether this rule is held also to the elements of the fairly lower atomic numbers, it seems to be permissible about down to Mn.

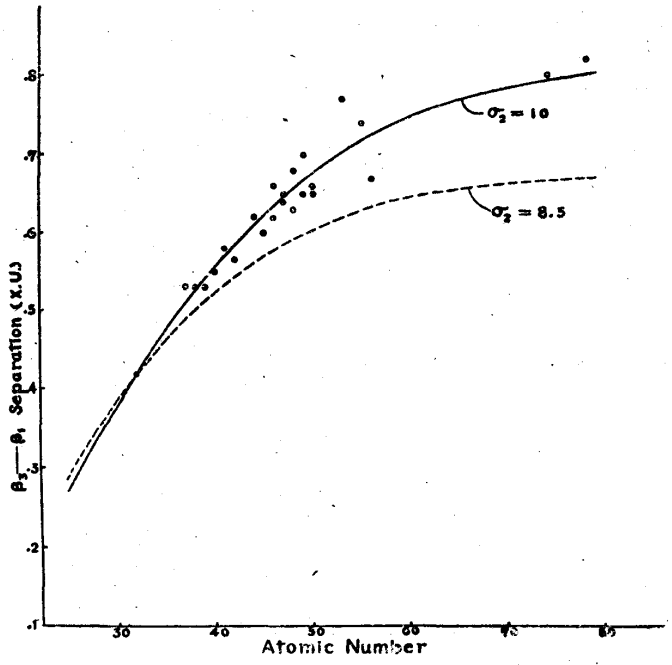

Fig. 60. The relation between the $\beta_3 - \beta_1$ wave-length separations and the atomic numbers.

Next let us plot the points denoting the relation between the measured values of the wave-length separaton $\beta_3 - \beta_1$ and the atomic numbers. They are indicated with small circles in Fig. 60. Among these points, the value for Ge(32) is that inferred from the writer's observation, those for Rb(37)~Ba (56) are taken from the text : Siegbahn, Spektroskopie der Röntgenstrahlen (1931) ; for W (74) and Pt (78) the values obtained by Kliever[22] are used.

Now, by adopting the value $\sigma_2 = 8.5$, and drawing a curve passing through the point for Ge, the one indicated with the dotted line is obtained showing tolerable deviations from the observed values. This will be probably caused by that Eq. (12) is an approximate formula in which the terms of the higher orders with respect to $(Z - \sigma_2)$ are omitted ; by putting for trial $\sigma_2 = 10$, the curve drawn in the solid line in the figure is obtained in good agreement with the observed values. From the theoretical point of view such treatment may be meaningless, but it seems to represent well the actual relation, so the wave-length separations are taken from this curve as listed in the following table.

Table 19. $\beta_3 - \beta_1$ separations (XU).

Element	Mn (25)	Fe (26)	Co (27)	Ni (28)	Cu (29)	Zn (30)	Ge (32)
$\beta_3 - \beta_1$ separation	0.28	0.30	0.32	0.34	0.36	0.38	0.42

(22) W.H. Kliever, Phys. Rev. **56** (1939), 387.

These values are adopted as the β_3—β_1 separations.

The resolutions are to be performed on these assumptions, the actual method, however, is quite trial and very difficult.

A resolution for Mn $K\beta$ which seems to be fairly satisfactory is shown in Fig. 61.

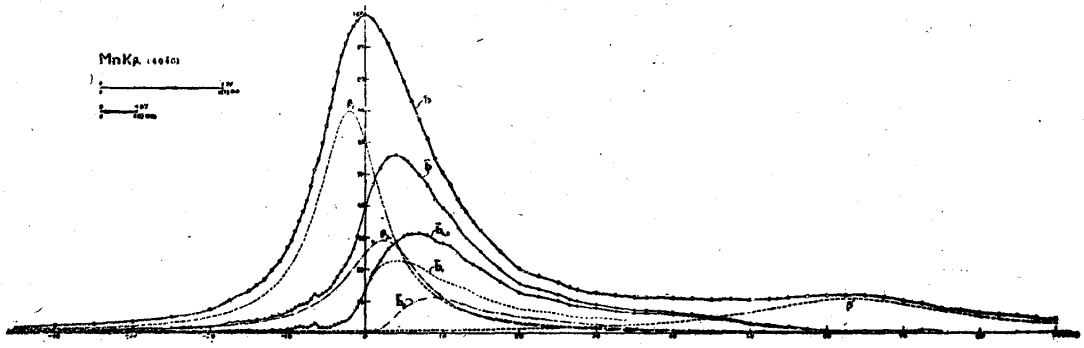

Fig. 61. The intensity distribution curve of Mn$K\beta$ and its component lines—(4040) reflection.

The procedure of the resolution is as follows: First, by subtracting the curves representing β_1 and β' from the observed curve $\boldsymbol{b}$, the curve $\overline{\boldsymbol{b}}$ is obtained. Next, the curve β_3 which satisfies the conditions (ii) and (iii) is subtracted from $\overline{\boldsymbol{b}}$, the rest part is $\overline{\boldsymbol{b}}_{1,3}$. $\overline{\boldsymbol{b}}_{1,3}$ is for trial resloved into $\overline{\boldsymbol{b}}_1$ and $\overline{\boldsymbol{b}}_3$, so that each point on $\overline{\boldsymbol{b}}_1$ to correspond to the point on $\overline{\boldsymbol{b}}_3$ equally distant with the β_1—β_3 separation, and the ratio of the corresponding ordinates to be 2 : 1. Accordingly the distance between the maxima of β_1 and $\overline{\boldsymbol{b}}_1$ and that of β_3 and $\overline{\boldsymbol{b}}_3$ become equal. These equal distances, denoted in eV (electron volt), are equal to the eV separation bewteen the maixmum ordinates of $\boldsymbol{a}_1$ and $\overline{\boldsymbol{a}}_1$ and also to that of $\boldsymbol{a}_2$ and $\overline{\boldsymbol{a}}_2$ in K_α and moreover the shapes of $\overline{\boldsymbol{b}}_1$, $\overline{\boldsymbol{b}}_3$, $\overline{\boldsymbol{a}}_1$ and $\overline{\boldsymbol{a}}_2$ are alike closely with one another. Thus, since $\overline{\boldsymbol{a}}_1$, $\overline{\boldsymbol{a}}_2$, $\overline{\boldsymbol{b}}_1$ and $\overline{\boldsymbol{b}}_3$ are equally related to $\boldsymbol{a}_1$, $\boldsymbol{a}_2$, β_1 and β_3 respectively, so $\overline{\boldsymbol{a}}_1$, $\overline{\boldsymbol{a}}_2$, $\overline{\boldsymbol{b}}_1$ and $\overline{\boldsymbol{b}}_3$ can be considered to be raised by certain common causes.

Though the results of the relsolution involve many questionable points, the general validity will be understood from the following illustrations. In fig. 61 the next values were taken for β_1 : the maximum value $B_1=70$, the half width $w_1=5.0$ mm, the abscissa of the maximum ordinate $x_1=-2.0$ mm. First let us make larger B_1 to $B_1=75$, leaving w_1 and x_1 as they were. β' is kept also as before. The corresponding graph is indicated in Fig. 62. Subtraction of β_1 and β' from $\boldsymbol{b}$ leaves $\overline{\boldsymbol{b}}$, and from this β_3, subjected to the assumptions (ii) and (iii), is to be subtracted. But the large width of β_3, results to make β_3 much larger than $\overline{\boldsymbol{b}}$ on the short wave-length side. On diminishing the width possibly, even with the maximum ordinate $B_3=47$, the half width $w_3=4.0$ mm, the abscissa of the maximum ordinate $x_3=2.2$ mm, there occurs negative values of $\overline{\boldsymbol{b}}-\beta_3$ at some places, so this selection is not suitable. Then on the contrary

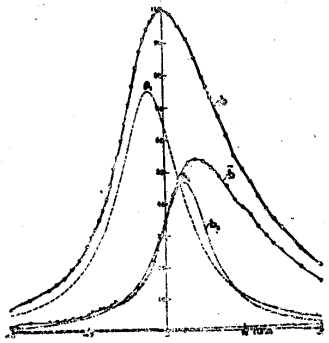

Fig. 62. Mn$K\beta$, the case $B_1=75$, showing the selection of β_1.

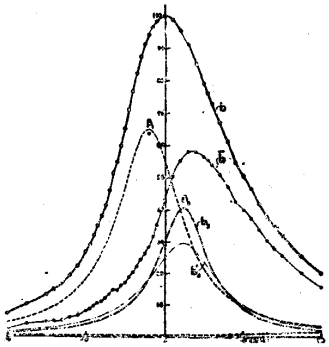

Fig. 63. Mn$K\beta$, the case $B_1=65$, showing the selection of β_1.

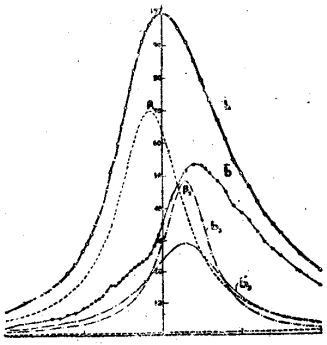

Fig. 64. Mn$K\beta$, the case $x_1=-1.5$ mm, showing the selection of β_1.

let us adopt the values $B_1=65$, $w_1=5.0$ mm, $x_1=-2.0$ mm. Fig. 63 indicates this case, in which two kinds of β_3 ($\boldsymbol{b}_3$ and $\boldsymbol{b}_3'$) are drawn as examples, both, however, differ too much from $\overline{\boldsymbol{b}}$.

Next, shifting the maximum ordinate of β_1 towards the right, let us see about the case $B_1=70$, $w_1=5.0$ mm, $x_1=-1.5$ mm (Fig. 64). In this case also both curves $\boldsymbol{b}_3$ ($B_3=48.6$, $w_3=3.3$ mm, $x_3=2.9$ mm) and $\boldsymbol{b}_3'$ ($B_3'=29.2$, $w_3'=6.0$ mm, $x_3'=2.9$ mm), the extremes of β_3, differ too much from $\overline{\boldsymbol{b}}$.

Conversely, by increasing x_1 negatively, consider the case when the values $B_1=70$, $w_1=5.0$ mm, $x_1=-2.5$ mm are adopted (Fig. 65). There appears a cavity on the left hand side of $\overline{\boldsymbol{b}}$, therefore unsuitable. As the extreme cases of β_3, two curves $\boldsymbol{b}_3$ and $\boldsymbol{b}_3'$ are drawn for trial. $\boldsymbol{b}_3$, at first sight, seems to agree with $\overline{\boldsymbol{b}}$ on the left side of it, the difference curve, however, becoming $\overline{\boldsymbol{b}}_{1,3}$, is accompanied by an unnatural cavity.

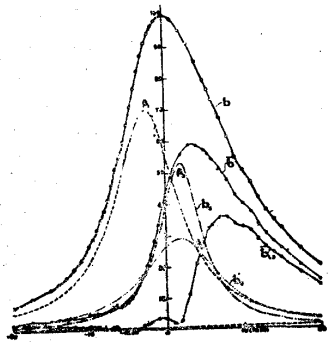

Fig. 65. Mn$K\beta$, the case $x_1=-2.5$ mm showing the selectlon of β_1.

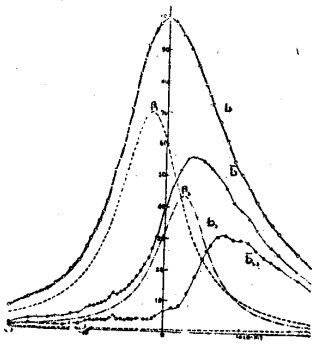

Fig. 66. Mn$K\beta$, showing the selection of β_3.

By the above mentioned the general validity of the determination will be recognized. Then in the next place let us consider about the selection of β_3 in Fig. 61. By way of example in Fig. 66 the case $B_3=45.95$, $w_3=4.0$ mm, $x_3=2.4$mm is shown. In this case the curve $\overline{\boldsymbol{b}}_{1,3}$ showing the difference $\overline{\boldsymbol{b}}$-$\beta_3$, exhibits an unnatural hump at the place $x=0$ and a cavity at $x=2$, therefore the selection indicated in Fig. 61 is more plausible after all.

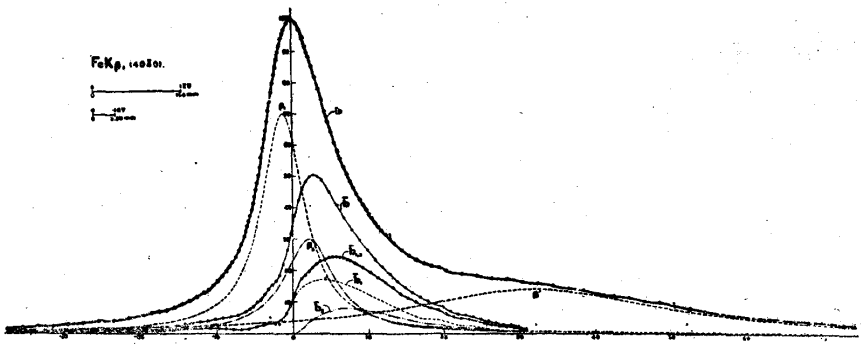

Fig. 67. Intensity distribution curve of Fe$K\beta$ and the resolved components —(40$\bar{4}$0) reflection.

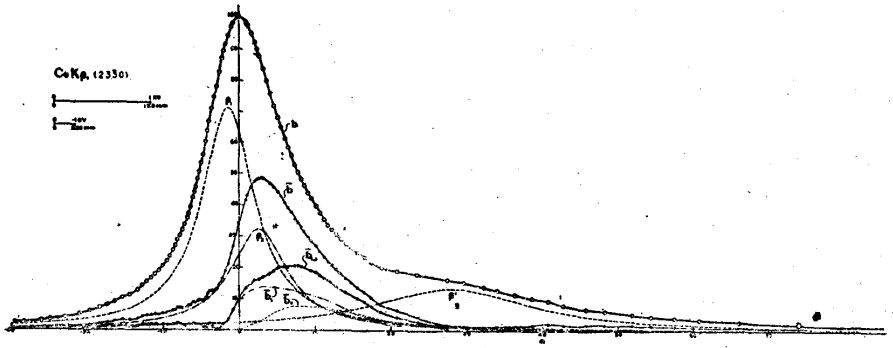

Fig. 68. Intensity distribution curve of Co$K\beta$ and the resolved components —(23$\bar{3}$0) reflection.

Similarly, resolutions were carried out for Fe and Co. These are shown in Figs. 67 and 68. The symbols are the same as in the case of Mn (Fig. 61).

For Ni, Cu, Zn and Ge, as in these elements there exists β_1' close by β_1 on the short wave-length side, the resolutions are more difficult. Consequently the resolutions for these are not yet perfect, but the general features are shown in Figs. 69 (Ni)~72 (Ge). In these cases there exist, besides β_1 and β_2, β_1' and β' (in the case of Ni one more component $\overline{\beta'}$), and for Ni, Cu and Ge one more component β_1'', for Zn $\overline{\beta_1'}$ (though not sure). Among these, in the case of Cu$K\beta$ shown by Fig. 70, there appears a cavity because of a white line (probably two white lines exist) at the place indicated with $\boldsymbol{p}$, so it was corrected in the form denoted by the dotted line, by comparing with a curve which is obtained by the reflection from another net plane.

The wave-lengths of the component lines as the results of the resolutions by the above stated procedures are generally in accord with the observed values already mentioned, though slight disagreements are unavoidable. Next, β_1' is very small for Mn, Fe and Co, increasing for Ni, the trace, however, is seen undoubtedly even for Mn~Co, and furthermore the tendency of augmentation with the atomic number is seen.

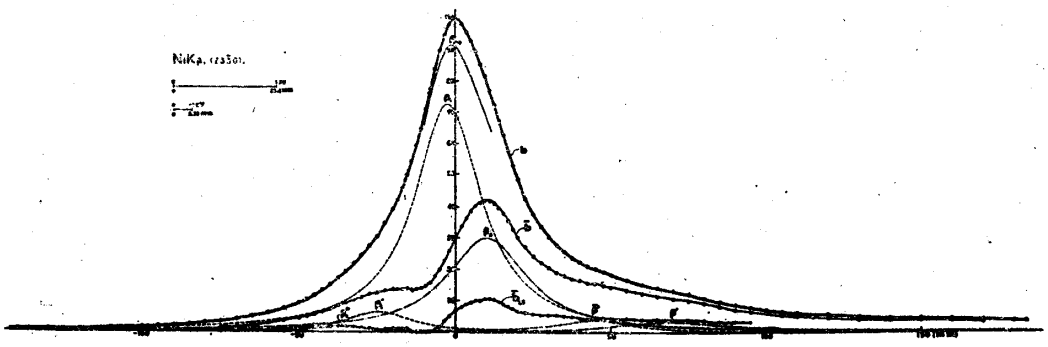

Fig. 69. The intensity distribution curve of Ni$K\beta$ and its resolved components —(23$\bar{3}$0) reflection.

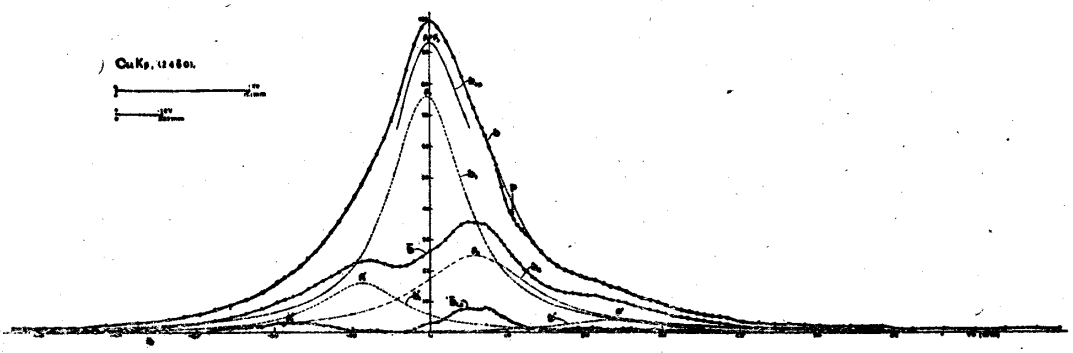

Fig. 70. The intensity distribution curve of Cu$K\beta$ and its resolved components — (24$\bar{6}$0) reflection.

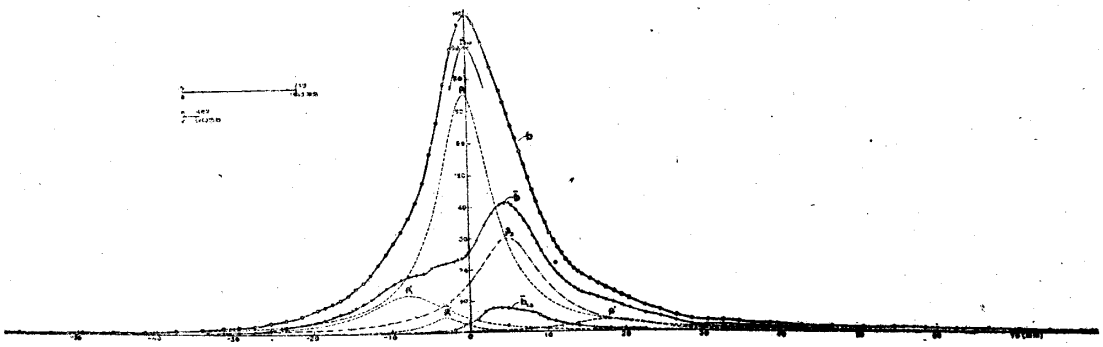

Fig. 71. The intensity distribution curve of Zn$K\beta$ and its resolved components—(23$\bar{6}$0) reflection.

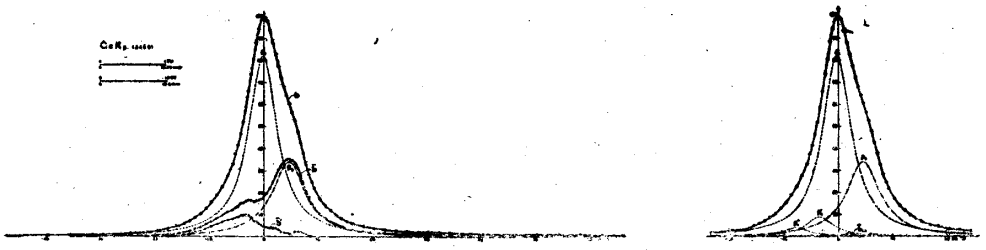

Fig. 72. The intensity distribution curve of Ge$K\beta$ and its resolved components —(24$\bar{6}$0) reflection.

(c) Correlation between the structures of $K_{\alpha_{1,2}}$ and $K_{\beta_{1,3}}$.

Let us represent the energy distributions of the asymmetric parts $\overline{a}_1$, $\overline{a}_2$ of α_1, α_2 respectively and also the rest parts $\overline{b}_1$, $\overline{b}_3$ of $\beta_{1,3}$ obtained by resolution into component lines, taking eV as the abscissae counted from the positions of the maximum ordinates of the resolved component lines α_1, α_2, β_1 and β_3 respectively. The ordinates, however, are expressed with the ratios of their intensities to the maximum values of α_1, α_2, β_1 and β_3 respectively. In this way we find a good similarity in the structures of α_1, α_2, β_1 and β_3 as shown in Fig. 73 (Mn), Fig. 74 (Fe) and Fig. 75 (Co). Therefore it can be considered that these components, the asymmetric parts or the rest parts, are raised by a certain common phenomenon. What will be the "common phenomenon"? Though it is not able to arrive at difinite conclusion, taking into account the fact that the asymmetric constructions of α_1 and α_2 are related with the progress of filling up of $3d$ ($M_{\text{IV,V}}$) -shell, they may be raised by the ejections of the $3d$-electrons. Then isn't it explained by the consideration, as already stated, that α_1, α_2, β_1 and β_3 are to be primarily of the classical dispersion shape, at the time of emission, however, the ejection

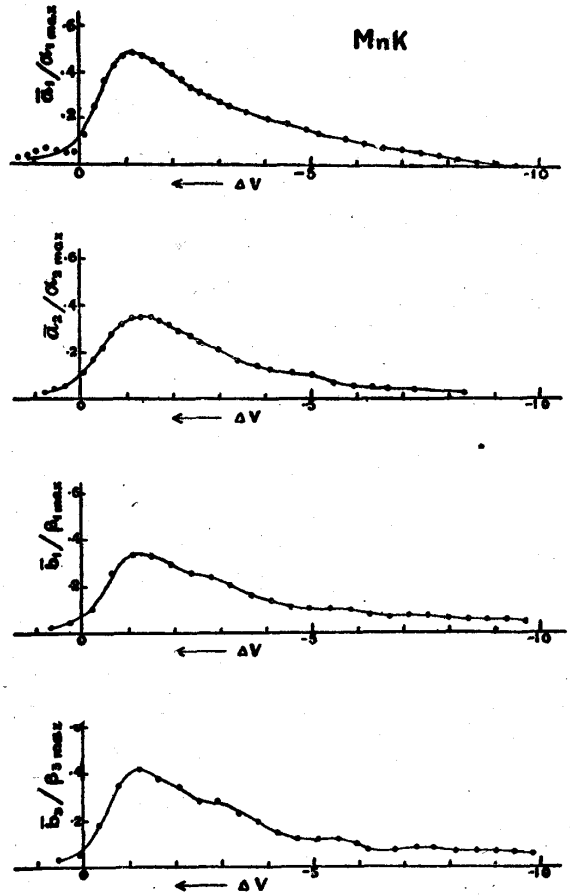

Fig. 73. Energy distributions of the asymmetric parts—MnK.

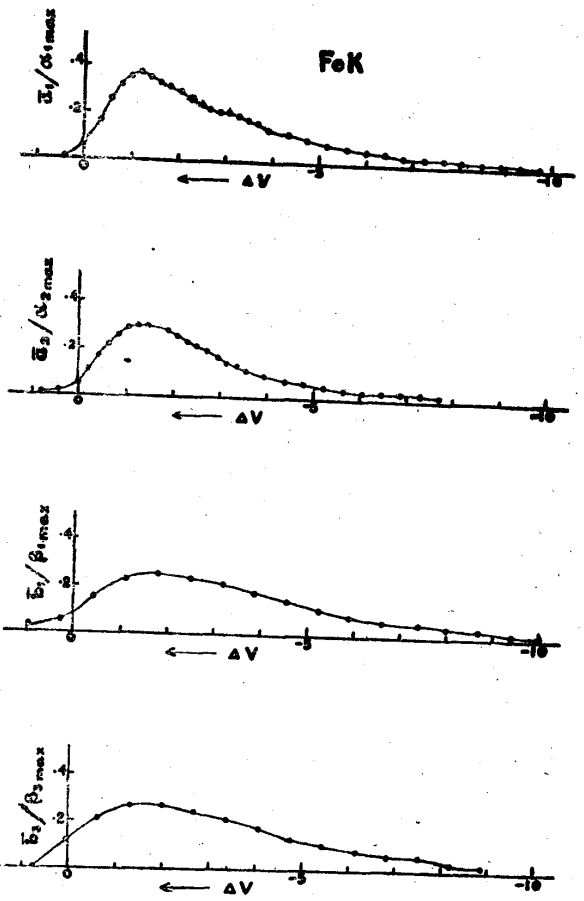

Fig. 74. Energy distributions of the asymmetric parts—FeK.

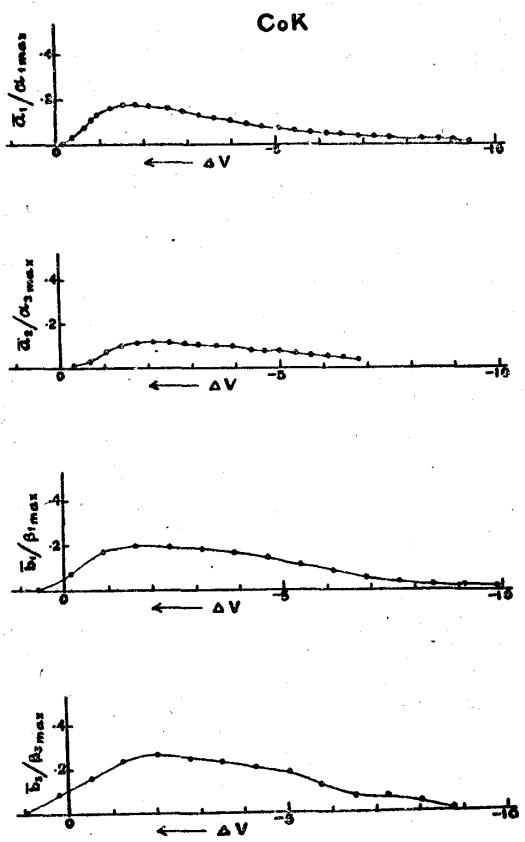

Fig. 75. Energy distributions of the asymmetric parts — CoK.

of 3d-electrons to the outest region of the atom is accompanied, and consequently the light quantum energy $h\nu$ of the emitted x-ray is reduced by the amount equal to the work spent for the ejection ? In this case the respective effects for the ejection of the 3d-electrons by α_1, α_2 β_1 and β_3 may be different with one another, but the above results show that they are almost equally effective for the ejection. Moreover, although the probability of double transitions of electrons like these are generally expectecd to be small, the above results show that in the cases of Mn and Fe, they amount to the order of magnitude comparable to that of the original line, which corresponds to the single transition. How to be explained these facts from the theoretical stand point ? They are the problems of the future. Splitting of $M_{\text{II, III}}$- and $L_{\text{II, III}}$-energy levels into still more levels on account of not filling up of 3d-shell are once to be considered, yet it seems insufficient to explain the above mentioned asymmetric parts with this reason alone, because its influence on $M_{\text{II, III}}$- and $L_{\text{II, III}}$-levels are not considered to be equal.

Next, comparisons are made for Ni, Cu and Zn. In these cases the resolutions of $\overline{\overline{b}}_{1,3}$'s into their respective two component lines for $K_{\beta_{1,3}}$'s were not achieved. They might be succeeded similarly by great efforts, it, however, was laid aside as it seemed to resort to artifice too much. Therefore the comparison is made between the energy distribution of $\overline{b}_{1,3}$, in which eV relative to the position of the maximum ordinate of the added curve of β_1 and β_3 (β_{1+3} in Figs. 69~71) is taken as the abscissa, and the asymmetric parts of α_1 and α_2. In this case the ordinates of $\overline{a}_1$. $\overline{a}_2$ and $\overline{b}_{1,3}$ are also denoted by the fractions divided by the maximum of α_1, α_2 and β_{1+3} respectively. Then the similarity of the asymmetric parts is recognized and the positions of the maximum values in eV are almost equal with one another as shown in Fig. 76 (NiK), Fig. 77 (CuK) and Fig. 78 (Zn K). For Ge, not indicated in the figure, the asymmetric parts of $K_{\alpha_1}$and K_{α_2} are very small, as shown in Fig. 56. Similar result is obtained for $K_{\beta_{1,3}}$ ($\overline{b}_{1,3}$ in Fig. 72) so that the similarity of the structures of K_α and K_β are regarded to be confirmed.

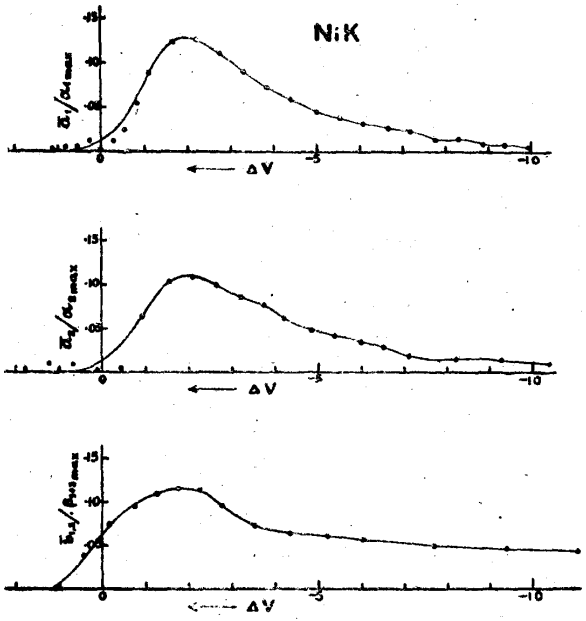

Fig. 76. Energy distributions of the asymmetric parts—Ni*K*.

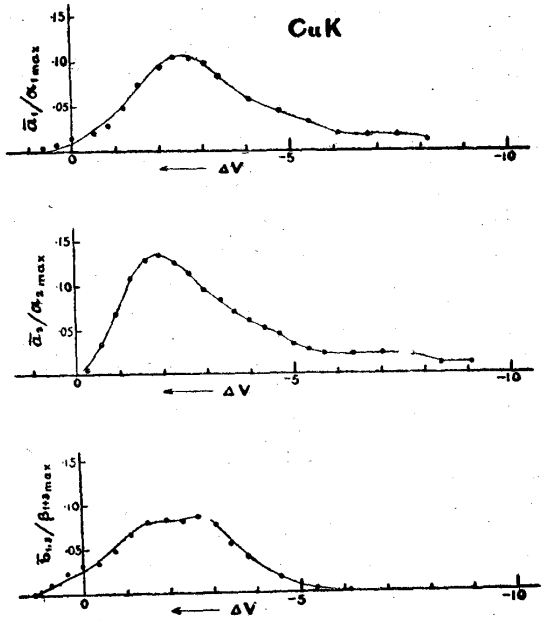

Fig. 77. Energy distributions of the asymmetric parts—Cu*K*.

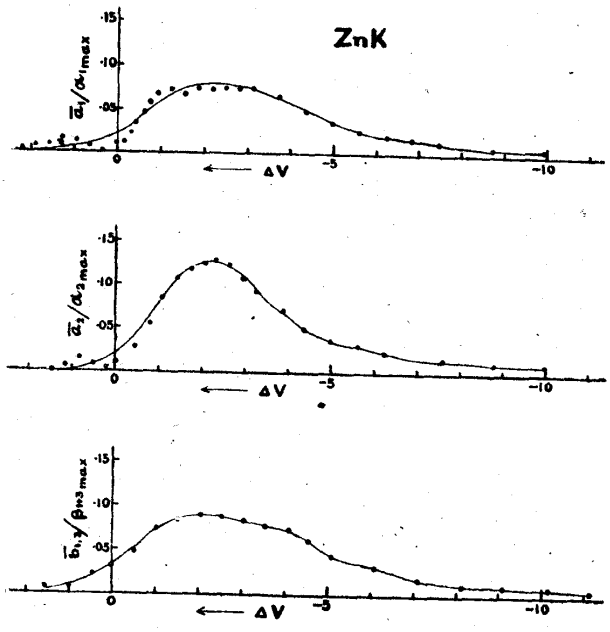

Fig. 78. Energy distributions of the asymmetric parts—Zn*K*.

(d) Wave-lengths of the resolved lines.

The wave-length corresponding to the maximum ordinates of the resolved lines thus obtained are as listed in Table 20.

(e) Ratio of the intensities of the resolved lines.

(i) Ratio of intensities K_{α_2} : K_{α_1} (ratio of areas).

In Table 21 the total intensity of α_2 is defined as the whole area of the resolved α_2, i.e. the sum of the areas of the classical shaped one ($\boldsymbol{a}_2$) and the asymmetric part ($\overline{\boldsymbol{a}}_2$). Similarly with α_1.

Among the observed values listed it is noted that those for Mn and Ni are very lagre. They may be reduced to some extent by supposing that the overlapping of α_1 and α_2 is more than the result of the resolution in this paper, but the explanation seems to be insufficient with it alone.

Table 20. Wave-lengths of the resolved lines (XU).

	Mn	Fe	Co	Ni	Cu	Zn	Ge
α_2	2101.35	1935.90	1789.17	1658.34	1541.20	1436.08	1255.43
α_1	2097.39	1932.02	1785.31	1654.51	1537.40	1432.24	1251.48
β'	1910.55	1755.73	1619.70	1499.22	1390.74	1293.86	
β'				1498.45			
β_3	1906.45	1753.18	1617.69	1497.39	1389.70	1292.96	1127.00
β_1	1906.17	1752.89	1617.37	1497.00	1389.34	1292.58	1126.60
β_1'						1292.40	
β_1'				1496.32	1388.85	1292.07	1126.33
β_1''				1495.93	1388.33		1125.96

Table 21. Ratio of intensities of $K_{\alpha_2} : K_{\alpha_1}$ (%).

	Mn	Fe	Co	Ni	Cu	Zn	Ge
$K\alpha_2 : K\alpha_1$	56	50.6	52.4	58.6	52.4	52.1	49.7

(ii) Ratio of intensities of the asymmetric part to the total resolved lines.

This ratio is, say for α_1 for example, the ratio of the area of the asymmetric part $\bar{a}_1$ to the sum of the areas of the symmetric part a_1 and the asymmetric part $\bar{a}_1$. Similarly with α_2.

Table 22. Ratio of intensities of the asymmetric part to the total resolved lines (%).

	Mn	Fe	Co	Ni	Cu	Zn	Ge
$\bar{a}_1 : (a_1+\bar{a}_1)$	57	31.2	17.5	13.8	8.9	8.0	1.5
$\bar{a}_2 : (a_2+\bar{a}_2)$	31	20.7	9.2	9.7	9.0	7.5	1.1

(iii) Ratios of intensities of the resolved lines to the total intensity of $\beta_{1,3}$ in $K_{\beta_{1,3}}$.

In the next table $\beta_{1,3}$ means the whole area of $\beta_{1,3}$ doublet line, and β_1, β_3, β', ... mean the areas of the respective resolved lines.

(f) The width at half maximum of the resolved line.

The widths at half-maxima of the resolved lines are listed in Table. 24. The width for CoK_{α_1} and CoK_{α_2} come out too large, this will be caused by that the quartz plate used in this experiment was not etched.

(g) Conclusion.

The results of the resolution above mentioned are summarized as follows:

(i) The spectrum lines K_{α_1}, K_{α_2} and $K_{\beta_{1,3}}$ may be regarded as to be composed

Table 23. Ratios of intensities of the resolved lines to the total intensity of $\beta_{1,3}$ in $K_{\beta_{1,3}}$ doublet line (%).

	Mn	Fe	Co	Ni	Cu	Zn	Ge
β_1 : $\beta_{1,3}$	37.5	30.9	40.6	49.9	52.7	52.4	60.9
β_3 : $\beta_{1,3}$	18.8	15.5	20.3	25.0	26.4	26.2	30.5
$b_{1,3}$: $\beta_{1,3}$	24.4	17.1	15.4	13.5	4.7	3.8	0.5
$\bar{\beta}'$: $\beta_{1,3}$				3.31			
β' : $\beta_{1,3}$	18.9	36.5	23.4	4.06	3.35	4.0	Trace
$\bar{\beta}_1'$: $\beta_{1,3}$						1.73	
β_1' : $\beta_{1,3}$				4.45	12.4	11.8	6.2
β_1'' : $\beta_{1,3}$				0.3	1.8		2.6

Table 24. Widths of the resolved lines (XU).

	Mn	Fe	Co	Ni	Cu	Zn	Ge
α_1	0.71	0.54	0.60	0.47	0.46	0.45	0.43
α_2	1.01	0.775	0.84	0.68	0.54	0.49	0.475
β_1	0.64	0.59	0.65	0.64	0.70	0.59	0.54
β_3	0.76	0.69	0.70	0.77	1.04	0.73	0.88
$\bar{\beta}'$				0.77			
β'	2.04	3.45	2.04	1.08	0.82	0.83	
$\bar{\beta}_1'$						0.305	
β_1'				0.64	0.76	0.83	0.50
β_1''				0.15	0.585		0.50

of component lines having the classical dispersion shapes. Some of the component lines are asymmetric in shape, but it is possible that these lines also may be regarded to be composed of several symmetric component lines.

(ii) There exists a correlation to a certain extent in the structures of the lines K_{α_1}, K_{α_2} and $K_{\beta_{1,3}}$. As to this cause the ejections of the outer electrons (3*d*- or 4*s*-electrons) will probably play an important rôle.

(iii) Performance of the resolution of this kind, indeed, enables the determination of the reasonable values of the component lines.

Summary.

The results of experiments are summarized as follows:

(i) By designing an apparatus to grind out a cylindrical surface having a large radius of curvature it is shown that a bent crystal spectrograph can be easily prepared.

(ii) Investigating the net planes of a quartz crystal which produce strong reflection, the dispersion for the characteristic x-rays of various elements are determined so that the study of x-ray spectra of these elements is facilitated.

(iii) A precise method for the comparative measurement of wave-length is given.

(iv) By designing and preparing auxiliary lenses for microphotometer, the effect of photographic grains on a microphotometric curve is reduced.

(v) Many weak lines for the elements Mn (25)~Zn (30) and Ge (32) are obtained and it is pointed out that some of these lines are mutually related.

(vi) It is confirmed that a fairly reliable result can be obtained in the intensity measurement by the microphotometric method.

(vii) K_{α_1}, K_{α_2} and $K_{\beta_{1,3}}$ are resolved into component lines.

(viii) As the result of (vii) it is shown that it can be considered that there exists correlation among the structures of K_{α_1}, K_{α_2} and $K_{\beta_{1,3}}$.

(ix) The result of (vii) indicates also that each resolved line may be regarded to be of the classical dispersion shape, and the reasonable values of wave-lengths, widths and intensities of every resolved lines can be obtained for the first time.

In conclusion the author expresses his gratitude to Prof. M. Yamada, a member of the staff of the Research Institute for Iron, Steel and Other Metals, for his guidance and stimulation and especially for his aid in preparing the spectrograph, and many thanks to Prof. J. Okubo who afforded convenience for using the microphotometer, and to Prof. I. Kobayashi and Dr. Mitsuru Satô for their interest and encouragement during the progress of this work, also to Prof. I. Koga and Assist. Prof. M. Tachibana then in the Tokyo Technological College for their kindness of preparing the quartz plates having the surfaces precisely parallel to the net plane and used in the spectrographs. This research had been carried out from 1936 to 1942 by the aid of the Foundation Hattori-Hôkô-Kwai, the author is thankful for offering the chance of this research.